Microbial Cell Factories

RESEARCH

Open Access

Unlocking marine microbial treasures: new PBP2a-targeted antibiotics elicited by metals and enhanced by RSM-driven transcriptomics and chemoinformatics

Syed Shams ul Hassan[1], JiaJia Wu[1], Tao Li[2*], Xuewei Ye[3], Abdur Rehman[4], Shikai Yan[1] and Huizi Jin[1*]

Abstract

Elicitation through abiotic stress, including heavy metals, is a new natural product drug discovery technique. In this research, three compounds 1, 2, and 6, were achieved by triggering zinc and nickel on marine *Sphingomonas* sp. and *Streptomyces* sp., which were absent in normal culture. Compound 5 was obtained for the first time from marine bacteria. All compounds showed potent antibacterial activity against *Staphylococcus aureu*s and bactericidal effect at 300 µm, but 6 was more active. The potent compound 6 production was further enhanced through response surface methodology by optimizing the condition consisting of nickel 1 mM ions, 20 mg/L sucrose, 30 mg/L salt and culture time 14 days. Under these conditions, the SM-6 production was enhanced with a yield of 6.3 mg/L, which was absent in the normal culture. Further transcriptome analysis of compound 6 unveiled its antibacterial activity on *S. aureus* by modulating heat shock protein genes, disrupting protein folding and synthesis, and perturbing cellular redox balance, leading to a comprehensive inhibition of normal bacterial growth. In addition, ADMET has shown that all compounds are safe for cardiac and hepatotoxicity. To determine the anti-bacterial mechanism, all compounds were docked with PBP2a and DNA gyrase enzyme, and TLR-4 protein for predicting vaccine construct, and the best docking score was achieved against PBP2a enzyme with the highest score of −10.2 for compound 6. In-silico cloning was carried out to ensure the expression of proteins generated and were cloned using *S.aureus* as a host. The simulation studies have shown that both SM-6-PBP2a and TLR-4-PBP2a complex are stable with the system. This study presents a new approach to anti-bacterial drug discovery from microorganisms through heavy metals triggering and enhancing the compound production through response surface methodology.

Keywords Natural Products, Anti-bacterial, Transcriptome, Heavy metals, PBP2a, ADMET

*Correspondence:
Tao Li
litao@shvri.ac.cn
Huizi Jin
Kimhz@sjtu.edu.cn
Full list of author information is available at the end of the article

Introduction

Marine secondary metabolites represent naturally occurring compounds produced by a wide range of marine life, such as microorganisms, sponges, and corals [1, 2]. These metabolites have been proven to be potent anti-tumor, anti-microbial, anti-inflammatory, and anti-hypertensive agents [3, 4]. The intricate nature of marine secondary metabolites, coupled with the substantial biodiversity of marine organisms, poses challenges in isolating and characterizing their chemical structures. The study of marine secondary metabolites is a rapidly growing field of research, with scientists exploring the potential of these compounds to treat various diseases and address global health challenges. The discovery and characterization of new marine secondary metabolites and a deeper understanding of their biosynthetic pathways and ecological roles can potentially drive the development of new drugs and therapies to benefit human health and the environment [5].

Marine bacteria-derived antibiotics have shown promise in combating antibiotic resistance, primarily due to their unique structures and mechanisms of action, which differ from traditional antibiotics [6]. These compounds, sourced from marine environments, offer new avenues for drug development and could potentially bypass existing resistance mechanisms. Marine-derived antibiotics such as marinopyrroles, salinamides, abyssomicins, and anthracimycins have demonstrated activity against multidrug resistant pathogens such as methicillin-resistant *Staphylococcus aureus* (MRSA), by targeting novel bacterial processes, reducing the likelihood of cross-resistance with existing antibiotics. In addition, these compounds restore the activity of beta-lactam antibiotics against resistant bacteria, suggesting that combination therapies could be a viable strategy to overcome resistance. Marine bacteria-derived antibiotics represent a promising frontier in the battle against antibiotic resistance. Their novel mechanisms of action, diverse chemical structures, and potential for synergistic effects, and efficacy against biofilms make them valuable candidates for developing new therapies to combat resistant infections [7, 8].

Microorganisms play a pivotal role in the elemental cycling of heavy metals within their environments. Exposure to elevated concentrations of these metals has compelled microorganisms to develop various strategies for coping with and adapting to these stressors [5]. The presence of heavy metals can influence microbial metabolism by modulating the expression of genes associated with secondary metabolism, leading to the production of unique metabolites with potential applications in biotechnology. Nevertheless, the precise mechanisms through which heavy metals trigger the synthesis of secondary metabolites in microorganisms remain inadequately understood [9, 10]. Recent strides in molecular and chemical biology have facilitated the examination of the molecular and biochemical pathways involved in these processes. A more comprehensive comprehension of how microorganisms react to heavy metals in their habitats holds significant implications for bioremediation, environmental surveillance, and exploring novel bioactive compounds for various biotechnological purposes.

Response surface methodology (RSM) is a statistical approach used to model and optimize complex systems, processes, and products. RSM is a powerful tool for designing experiments, predicting outcomes, and identifying optimal settings for process variables. RSM is widely used in fields such as engineering, manufacturing, chemistry, and agriculture, where the goal is to optimize product quality, reduce costs, increase efficiency, or maximize performance. The methodology involves designing experiments, collecting data, fitting mathematical models to the data, and using these models to explore the response surface, representing the relationship between the response variable and the independent variables. RSM has several advantages over traditional experimental design methods, including its ability to account for the effects of multiple factors, model non-linear and interactive effects, and identify optimal settings for process variables. Overall, RSM is a valuable tool for anyone seeking to optimize and improve their products, processes, or systems through effective experimental design and data analysis [11].

In our research, we have isolated a number of new antibiotics from multiple bacterial strains through different kinds of heavy metals, and the potent compound production was further enhanced by RSM. The antibacterial activity of all the compounds was tested against multiple gram-positive and gram-negative pathogens. ADMET, molecular docking, and simulations were also performed to determine the best compounds. Transcriptomic analysis was also performed for the best compound to evaluate its in-depth mechanism behind anti-bacterial activity.

Materials and methods

General

High-performance liquid chromatography (HPLC) system was used with a set of Waters 996 Photodiode Array Detector and a Waters 717 plus Autosampler (SHIMADZU LC-2010AHT, 1290 infinity II HDR-DAD Agilent), U.V (SHIMADZU UV-2550), the column used was Zorbax SB-C18, 5 µm, 4.6×250 mm by Agilent. On a Bruker AVANCE DRX 500 NMR spectrometer with TMS as an internal standard, ^{1}H NMR (500 MHz) and ^{13}C NMR (125 MHz) spectra were measured at 25 °C.

The heavy metals were purchased from Sangon, Biotech Shanghai, China.

Soil sample collection

The marine sediment samples were procured from locations near the sea shores in Ningbo city, Fenghua, Zhejiang, approximately 100–200 m inland. These samples were gathered from both polluted and unpolluted areas adjacent to the coastline. The polluted areas were contaminated with ship oils and waste from factories. The samples were then taken to the lab, immediate isolation was started, and the remaining samples were kept at 4°C in the refrigerator (Figure S1).

Isolation and storage of strains

In this study, a 10–1 dilution of a fresh soil sample C2, weighing approximately 1–2 g, was prepared by adding simulated seawater to pre-sterilized glass vials. The mixture was then subjected to sonication for 1 min to release microorganisms that were attached to the soil particles, followed by shaking for 15 min at room temperature. Subsequently, serial dilutions up to 10–2, 10–3, and 10–4 were made, and nystatin (0.05 g/L) was added to the pre-prepared Potato dextrose agar (PDA) media to prevent fungal contamination. 100 µl aliquots of each dilution were inoculated on the media and spread with pre-sterilized spreaders. The plates were then incubated at 28 °C for 15–20 days, and purified colonies of bacteria were collected and stored on agar media at 4 °C.

Molecular characterization

The DNA extraction was performed using the Omega Mag-Bind Soil DNA kit (M5635-02), following the manufacturer's instructions from pure cultures of bacterial isolates (C2-110, C2-94, and C2-73). Subsequently, the concentration and purity of the DNA were evaluated using electrophoresis on a 1% agarose gel. The V3-V4 variable region of the 16S rRNA gene was amplified using the universal primers 338F (5'-ACTCCTACG GGAGGCAGCA-3') and 806R (5'-GGACTACHVGGG TWTCTAAT-3') [12] and paired-end sequenced at Sangon Biotech (Shanghai). The DNA sequences were demultiplexed using Quantitative Insights into Microbial Ecology (QIIME) version 1.7.0 [13]. Sequences exhibiting poor quality and containing uncertain nucleotides were eliminated. The paired-end sequences were combined utilizing the Fast Length Adjustment of Short Reads (FLASH) tool [14]. Following this, chimeric sequences were excluded, and the remaining sequences were clustered into operational taxonomic units (OTUs) with 97% sequence similarity utilizing the UPARSE algorithm [15]. The taxonomic identity of the OTUs was determined by comparing them to the SILVA138 SSU rRNA reference database [16]. Sequence counts were standardized to the sample with the fewest sequences. The Chao1 and Shannon indices were computed using QIIME and visualized using R version 2.15.3.

Metal stress and normal cultivation

The growth of three bacterial strains, C2-110, C2-94, and C2-73, were tested with and without heavy metals in 500 mL Erlenmeyer flasks containing 250 mL PDB media, maintained at 28 °C on a rotatory shaker operating at 180 rpm for ten days. As a control, two flasks underwent standard batch growth of the variants above (C2-110, C2-94, and C2-73) to ensure the accuracy of the results. The C2-110, C2-94 and C2-73 stressed culture medium were supplemented with different $ZnSO_4$, $NiCl_2$, $CrCl_2$ and $MnCl_2$ concentrations at 0.5, 1, 2, and 4 mM, respectively. Ethyl acetate (EtOAc) was added three times at the same concentration to extract the metabolites from the mycelium. The EtOAc extract was then evaporated in a rotary evaporator to obtain the secondary metabolites extract. A gummy residue was then subjected to the next phase separation technique through HPLC.

Extraction and isolation through HPLC technique and refinement of stress metabolites

The reversed-phase HPLC–UV analysis was conducted using an HPLC system equipped with a C18 column to separate the chemical compounds. The HPLC method employed wavelengths of 210 nm and 254 nm. The gradient elution consisted of a mixture of H_2O and MeOH, ranging from 10 to 100% MeOH over 0 to 30 min, followed by 100% MeOH from 30 to 40 min. The flow rate was maintained at 0.1 mL/min throughout the analysis. Subsequently, the stress-induced metabolite was isolated using Prep-HPLC, operated at a constant flow rate of 9 mL/min with a consistent mobile phase composition. Ethyl acetate (EtOAc) was utilized in three separate extractions, each with a volume of 250 mL, to extract the 15-L fermented broth containing strains C2-110, C2-94, and C2-73. Following solvent evaporation, the resulting crude residue was dissolved in methanol and centrifugated at 120,000 rpm for ten minutes before undergoing analytical HPLC analysis. In the initial screening phase, HPLC analysis was performed using a gradient of H_2O and MeOH ranging from 10 to 100% for 30 min. Subsequently, new or elevated peaks were observed at varying concentrations in the HPLC chromatogram. The compound of interest was then purified using preparative HPLC with a constant mobile phase consisting of a selected eluent mixture of methanol and water. For structural elucidation, the purified compound underwent 1D NMR analysis, including ^{1}H NMR, ^{13}C NMR, and

DEPT135. The structure of the metal-induced compound was determined through 1D NMR spectroscopy.

Antibacterial assay

The antibacterial assay of all stressed metabolites were evaluated against ten pathogenic gram-positive and gram-negative bacteria. The six pathogenic bacteria were purchased from ATCC and others were hospital-acquired with the following accession number: *Escherichia coli* ATCC25922, *Enterococcus faecalis* ATCC51299, *Staphylococcus epidermidis* ATCC12228, *Staphylococcus aureus* (SA) ATCC29213, methicillin-resistant *Staphylococcus aureus* (MRSA) ATCC43300, *Salmonella gallinarum* ATCC14028, *Klebsiella pneumonia* (clinical strain), *Acinetobacter baumannii* ab201A (clinical strain), *Proteus mirabilis* PM70 (clinical strain), and *Riemerella anatipestifer* WH59 (clinical strain). The bacterial suspension was shaken to the logarithmic growth phase and diluted to 0.5 McFarland standard, which is approximately an OD value of 0.1. The compound concentration was 10 mmol/L, and the experimental compound concentration was 400 µM. First, 92 µL of MH broth was added to each well of a 96-well plate, followed by 8µL of the compound in order. Finally, 100µL of the diluted bacterial suspension was added and mixed well. Each strain was tested in duplicate with each compound. The plate was incubated at 37 °C for approximately 24 h in an incubator. The absorbance was measured at 600 nm using an ELISA reader. The positive control drug was ciprofloxacin with a concentration of 6 µg/mL.

Medium optimization for enhanced production of stress metabolite through response surface methodology

Experimental design

A Box-Behnken Design (BBD) was used to evaluate the effect of four factors, namely heavy metal (HM), sucrose (SU), time (T), and salt (SA), on the response variables of compound production. Prior to commencing optimization experiments, it is essential to identify the key factors influencing the quality of the resulting outcomes. The selection of variable stages was based on their significant impact on production, ranging from minimum to maximum effects. Additionally, each stage was tested at both lower and higher ends to assess their influence comprehensively [11]. Each factor was evaluated in 4^4 factorial designs, as shown in Table 1.

Experimental procedure

A total of 29 experiments were conducted according to the BBD matrix with three replicates at the center point to assess the response variables. The experiments were performed in a random sequence to mitigate the influence of external variables. All other factors, such as temperature and volume, were consistent throughout. The response variables were analyzed using Design-Expert software (version 12.0.3, Stat-Ease Inc., Minneapolis, USA).

Table 1 Levels of tested parameters for Box–Behnken design

Symbol	Independent factors	Unit	Levels		
			Low	Mid	High
A	Time (T)	Days	7	14	21
B	Sucrose (SU)	mg/L	15	20	25
C	Salt (SA)	mg/L	25	30	35
D	Heavy metal (HM)	mM	0.5	1.0	1.5

The data obtained were analyzed using the following second-order polynomial equation:

$$Y = \beta_0 + \Sigma\beta_i X_i + \Sigma\beta_i X_{ii}^2 + \Sigma\beta_{ij} X_i X_j$$

where, Y is the response variable, β0 is the intercept, βi is the linear coefficient, βii is the quadratic coefficient, and βij is the interaction coefficient between the ith and jth factors. X1, X2, X3, and X4 are the coded values of T, SU, SA, and HM, respectively.

Transcriptome analysis

RNA sequencing

SA bacterial cells were treated with SM-6, followed by a subsequent collection for transcriptomic analysis. Following an incubation period of 60 min at a temperature of 37 °C, the cells were subjected to centrifugation. Total RNA extraction, removal of ribosomal RNA, cDNA synthesis, RNA library preparation, transcriptome sequencing, and bioinformatic data analysis were conducted employing the Illumina HiSeq platform.

DEGs screening and bioinformatics analysis

The original sequence data underwent quality analysis using the FastQC software. Subsequently, the NGSOC and Bowtie2 software were used to filter out low-quality data and acquire high-quality clean data. Finally, calculations were performed on the filtered Clean Data. Differentially expressed genes (DEGs) were identified using the edgeR package (v3.14.0). The obtained results underwent adjustment of the *p*-values using the Benjamini–Hochberg method to control the false discovery rate. DEGs were determined based on p-value < 0.05 and $|\log_2 FC$ (fold change)$| > 1.0$.

To annotate the DEGs, a GO enrichment analysis (http://www.geneontology.org/) was conducted to categarize these DEGs to three structured terminologies, including biological process (BP), molecular function

(MF), and cellular component (CC), by Goatools software. Furthermore, KEGG enrichment analysis (http://www.genome.jp/kegg/) was conducted by using R scripts to identify the principal categories of DEGs.

ADMET

ADMET (Absorption, distribution, metabolism, excretion, and toxicity) evaluations are imperative in assessing the viability of any compound as a potential drug candidate. To acquire the ADMET properties of the stress compounds, the online tool Swiss ADME (http://www.swissadme.ch/index.php) was utilized [17].

Prediction of cardiac toxicity

The prediction of cardiac toxicity, which is often associated with fatal cardiac arrhythmias stemming from the blockage of hERG K+channels, the freely accessible online service pred-hERG 4.2 (http://predherg.labmol.com.br) was employed. This tool aids in the early identification of potential hERG blockers and non-blockers, thereby contributing to the mitigation of cardiac risks associated with drug development [18].

Molecular docking analysis

Ligand and protein preparation

Molecular Docking analysis was performed to predict the binding affinity of stress metabolites with target proteins. In the current study, Autodock vina 1.1.2 in PyRx 0.8 was employed for docking analysis of the three-dimensional structure of proteins against active ingredients. For proteins, their 3D structure was downloaded from the RCSB PDB (www.rcsb.org). Following the download, all solvent molecules present in the protein structures were carefully removed to avoid any interference during docking simulations. Heteroatoms and already attached ligands were carefully removed from the protein structure. Subsequently, the proteins were protonated to add hydrogen atoms, ensuring that all ionizable groups were in their correct ionization states at physiological pH of 7–7.5. Finally, energy minimization was performed on each protein structure. This process optimizes the conformation of the proteins by reducing strain and eliminating any unfavorable interactions, thereby ensuring that the proteins are in a stable and realistic conformation for accurate docking results. On the other hand, the SDF formats of compounds were prepared by Chemiodrad were exposed to Openwhich is Babel, available in PyRX for energy minimization. To achieve a stable conformation, an optimization algorithm known as conjugate gradient descent was utilized in conjunction with the Universal Force Field (UFF) as the energy minimization parameter. Further, 2000 steps were set for energy minimization and the minimization was set to stop at an energy difference of < 0.01 kcal/mol. The energy-minimized ligands were converted to.pdbqt format docking. Subsequently, the site finder tool within the Molecular Operating Environment facilitated the identification of binding pockets on the target proteins, while PyRx software facilitated the docking of the core targets with active compounds. Later, the docking was performed using PyRx 0.8 to calculate binding energies of ligand molecules with target proteins. Autodock vina utilized an empirical scoring function to determine the affinity of protein-compound binding, which was calculated by aggregating contributions from various individual terms. The docked complex with the lowest root mean square deviation (RMSD), was considered the optimal complex, and the binding energies among ligand and target protein were evaluated based on their affinity. A good binding strength was indicated by a value < -5.00 kcal/mol, while a value < −7.00 kcal/mol indicated very good affinity. Finally, docked complexes were visualized by Discovery Studio, PyMOL, and ChimeraX programs.

Protein–protein docking

Human Toll-like receptors (TLRs), including the three-dimensional structure of TLR4, were obtained from the Protein Data Bank (PDB ID: 2z65). Refinement of the receptor model was carried out using the Galaxy refine server, with subsequent removal or exclusion of any ligands associated with the retrieved structures. To explore the interaction profile between the vaccine and TLRs, molecular docking analysis was conducted using the HADDOCK 2.0 protein–protein docking server. This server generates cluster scores based on rigid docking, aiming to minimize pairwise RMSD energy between conformations. The final version of the vaccine-TLRs complex model was selected based on the lowest energy weight score and its constituents. Subsequently, this model was visualized using the UCSF Chimera v1.10.1 system.

In silico cloning and codon optimization

Codon optimization is a technique used to enhance the efficiency of translating foreign genes in a host organism when there are differences in codon usage between the two organisms. Following a thorough evaluation of the properties and immune response of the RIEAN Multifunctional fusion protein, codon optimization was conducted, followed by in silico cloning. To ensure compatibility with the commonly employed prokaryotic expression system, specifically *S. aureus*, the Java Codon Adaptation Tool (http://www.jcat.de/) was utilized for codon optimization.

The Codon Adaptation Index (CAI) and GC (guanine and cytosine) content were analyzed. Sticky ends of

HindIII and BamHI restriction enzymes were incorporated to facilitate restriction and cloning at the start/N terminal and end/C terminal of the modified target sequence, respectively. Additionally, the modified nucleotide sequence of the target sequence was cloned into the *S. aureus* strain USA300 pET30a (+)-Tev and pCC1 vectors using the SnapGene tool (https://www.snapgene.com/) to ensure its in vitro expression.

Molecular docking simulations

Molecular Dynamics Simulation (MDS) analysis was performed to assess the stability of ligand–protein interactions. The structural transitions of the macromolecules and their functional significance within the complex were investigated through MD simulations. MD simulations of the small molecule (SM) and targeted proteins were conducted for 100 ns (ns) using the Desmond v:3.6 module of the Schrödinger suite in New York, USA module [19]. The initial structures of the MD simulations were prepared according to an established protocol, with protein atoms placed 10 angstroms away from the simulation box. The complex derived from MD served as the initial structure for subsequent MD simulations. The ligand-receptor complex was minimized and optimized using the Wizard of Maestro, and a solvent standard TIP3P with an orthorhombic box was selected for the systems using the System Builder tool. The OPLS 2005 force field was employed for simulation analysis, and physiological conditions were adjusted by adding 0.15 M NaCl [20]. All MD simulations were conducted under constant temperature (300 K) and pressure (1 atm) using an NPT ensemble. MDS trajectories were recorded at intervals of 100 picoseconds (ps). RMSD, RMSF, Rog, and SASA were calculated to measure the stabilities during simulations. Each complex underwent three separate MDS runs under identical parameters.

Results

Molecular characterization of bacterial strains

The molecular characterization of the bacterial strains C2-110, C2-94, and C2-73 was characterized by Sangon biotech (Shanghai). According to the 16S sequencing, initially multiple phyla were detected in the strain, and a single-sample multi-level species composition map visually displayed the annotation results of strain C2-110, C2-94, and C2-73 (Fig. 1). During the taxonomic comparison results of C2-110 and C2-94, only the classification of dominant species was selected, and the most dominant species were proteobacteria and actinobacteria. After that, further analysis showed high abundance for the class alpha proteobacteria, family *Sphingomonadaceae* and genus *Sphingomonas,* and species *Sphingomonas* (Fig. 1a, c). All the nucleotide and genomic sequences were uploaded to the NCBI depository with the accession no DQ147571. For C2-73, the higher abundance was shown for the class actinobacteria, sub-class actinobacteridae, order actinomycetales, sub order *streptomycineae*, family *Streptomycetaceae* and genus *Streptomyces* and *species Streptomyces* (Fig. 1b, d). All the nucleotide and genomic sequence was uploaded to the NCBI depository with the accession no DQ513513. Further, GraPhlAn plotted a visualization of taxonomic and phylogenetic information (Fig. 1c, d). In the center of the figure is a taxonomic tree with an abundance greater than 1%, with different colors representing different phyla and dot sizes representing abundance. Points with an average abundance greater than 1% are indicated by purple squares, and conversely by an inverted orange triangle. The outer ring is a heat map, the darker the color, the higher the abundance. The outermost ring is a histogram, and the higher the column, the higher the abundance. Inside the circle blue lines shows actinobacteria and green lines shows proteobacteria (Fig. 1c). Visualization of most dominant species, proteobacteria, actinobacteria and Firmicutes classification and phylogenetic information of C2-73 (Fig. 1d).

HPLC evaluation of secondary metabolites of metal treated and untreated extracts

C2-110

Experiments were conducted to assess the effects of elution mode, mobile phase composition, detection wavelength, and column temperature to identify the optimal HPLC conditions for purifying the stressed metabolite of C2-110. Strain C2-110 was cultured in the normal and metals-containing fermentation media. Initially four different types of metals including $ZnSO_4$, $NiCl_2$, $MnCl_2$ and $CrCl_2$ were selected (Figure S2). All 4 metals with their four initial concentrations 0.5, 1, 2 and 4 mM were chosen as initial elicitors to evaluate the bacterial strain C2-110 potential against these metals in PDB medium at 160 rpm for 12 days at 28 °C. The changes in the metabolic profile resulting from exposure to metal ions were confirmed by establishing several experimental conditions. These included one medium without any metal ions as a blank reference, one medium without bacteria serving as the metal control, and four groups of media with varying ionic concentrations ranging from 0.5 to 4 mM. All the metals responded towards C2-110 in different concentrations but the best outcome was achieved with the presence of $ZnSO_4$ at 0.5 mM. Two new peaks were elicited at this concentration at 10.3 and 14.8 min which were totally absent in the normal culture and also in the other concentrations, while two other peaks at 20.7 min and 22 min elicited higher as compared to the normal culture, which here by shows that this condition

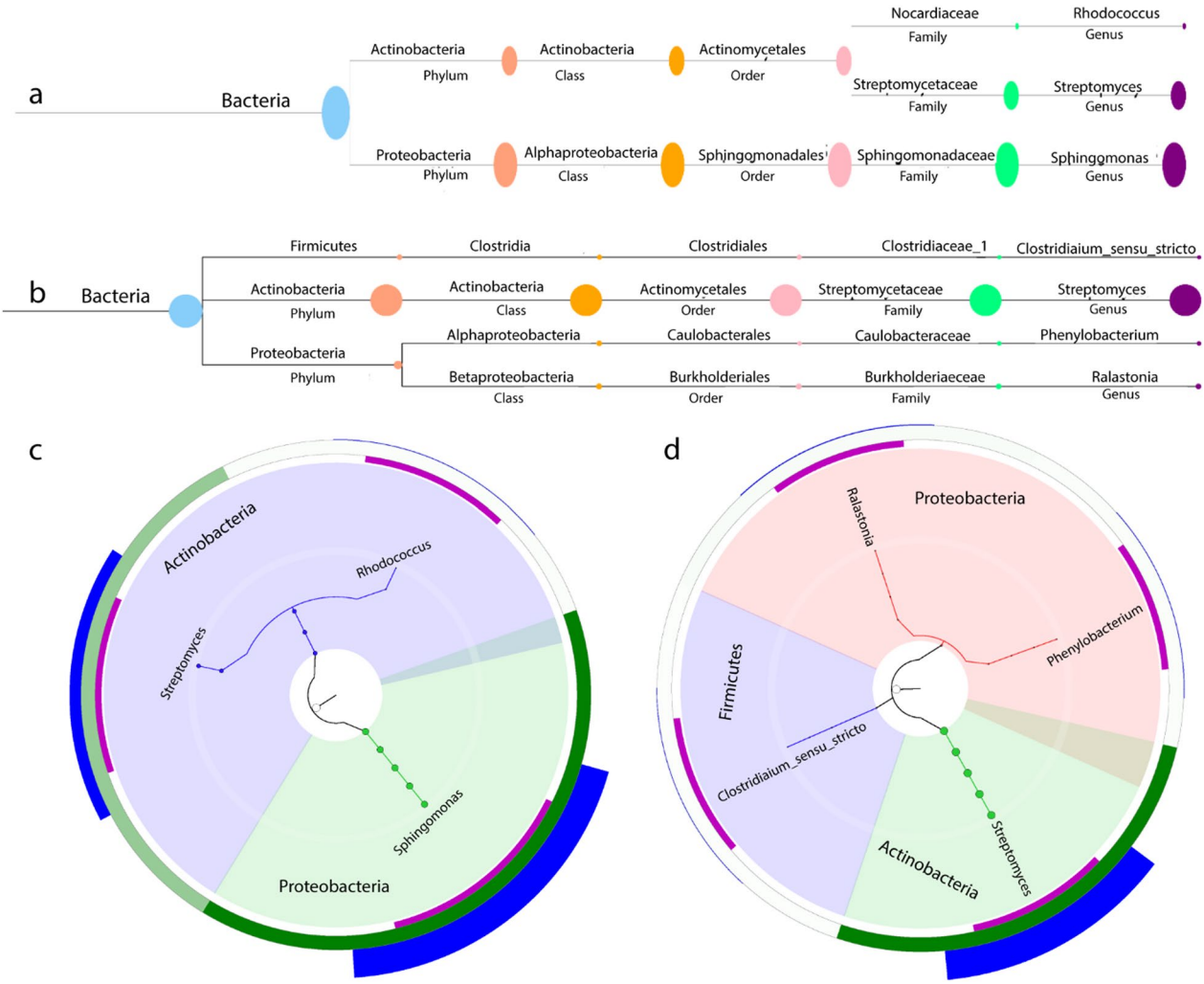

Fig. 1 **a** C2-110, C2-94 **b** C2-73**.** Single-sample classification system composed of a tree view. The different colors in the figure represent different classification levels, from left to right, the size of the circle represents the abundance of species, and near the fulcrum are the name of the classification and its corresponding abundance value. **c** Visualization of most dominant species, proteobacteria and actinobacteria classification and phylogenetic information of C2-110 and C2-94. **d** Visualization of most dominant species, proteobacteria, actinobacteria and Firmicutes classification and phylogenetic information of C2-73

not only triggered a new peak but also enhanced the production of other peaks compared to normal (Figure S2a). The presence of $NiCl_2$ in the culture of C2-110 did not elicit any new peak but with the 2 mM and 4 mM presence enhanced the length of two peaks at 18 min (Figure S2b). The addition of $MnCl_2$ in the media also enhanced the same peak like $NiCl_2$ at 18 min but also enhanced another peak at 20 min at 2 mM and 4 mM concentration (Figure S2c). The last metal $CrCl_2$ haven't any strong effect on bacteria but a new peak was also elicited at 1 mM at 14.4 min same like $ZnSO_4$ (Figure S2d). Over all on the basis of all HPLC chromatograms $ZnSO_4$ at its 0.5 mM concentration was selected for large-scale culture. A total number of two stress-induced compounds were purified and identified through 1D NMR (^1H, ^{13}C and DEPT135) [21] as pyrrole-2-carboxylic acid (SM-1) (t_R = 10.3 min) and streptazolin (SM-2) (t_R = 14.8 min) (Fig. 2).

C2-94

The procedure for metals treated and untreated strain C2-94 was the same like C2-110. Two metals $MnCl_2$ and $CrCl_2$ didn't exhibit any changes to the C2-94 pattern, but metabolomics changes were observed with $ZnSO_4$ and $NiCl_2$ (Figure S3). C2-94 strain showed metabolomics change with addition of $NiCl_2$, The changes were observed in almost all four concentrations, but 1 mM have shown tenfold enhancement

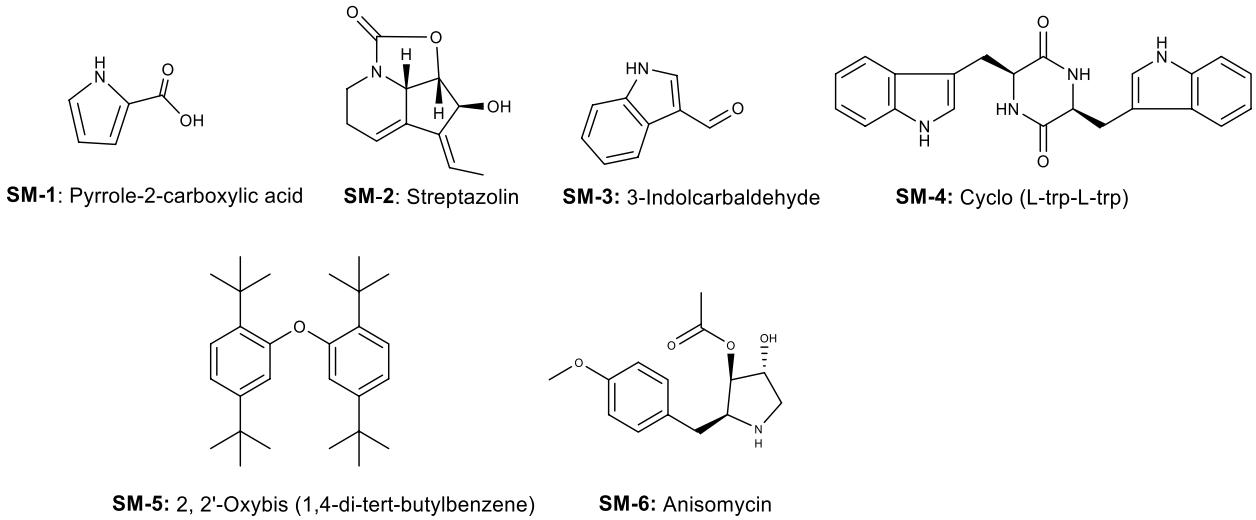

Fig. 2 Chemical structures of SM's (**1-6**)

of peaks at 16 and 18 min. The supplementation of $ZnSO_4$ in the culture media of C2-94 did not show any new peak but the peak at 15 min was enhanced in 0.5–2 mM, but at 4 mM, the peak started to decline, which can show that this concentration was toxic for the bacteria. After comparing the hplc results of all metals with C2-94, the best culture medium was selected as C2-94 with the addition of $NiCl_2$ 1 mM concentration. Only at this concentration, the two peaks at 15 and 18 min showed enhanced growth of tenfold as compared to blank. The peak at 16 min was purified and identified as sucrose, which was one of the supplement added to the medium. A total no of three compounds were purified and identified from the culture as 3-indolcarbaldehyde (SM-3) ($t_R = 15.1$), Cyclo (L-trp-L-trp) (SM-4) ($t_R = 18.3$) and 2,2'-oxybis(1,4-di-tert-butylbenzene) ($t_R = 26.3$ min) (SM-5) (Fig. 2).

C2-73

The procedure for metals treated and untreated strain C2-73 was the same like the previous. Except for $NiCl_2$, none of the metals showed any peak alterations and the change in metabolic pattern of $NiCl_2$ were seen. The best condition for a large culture was selected as 0.5 mM. During the addition of $NiCl_2$, one new peak was elicited at all concentration at 20.8 min which was totally absent in the normal culture and also declined at other concentrations. Over all on the basis of all HPLC chromatograms $NiCl_2$ at its 0.5 mM concentration was selected for large scale culture. The stress induced compound was purified and identified as anisomycin (SM-6) ($t_R = 20.8$ min) (Fig. 2).

Characterization of stress metabolites

Stress metabolite (SM–1)

Stress metabolite (SM–1) was isolated as a white powder. The molecular formula $C_5H_5NO_2$ was established from ESI–MS m/z 134 $[M+Na]^+$. ^1H NMR (CD_3OD-d_4, 500 MHz) showed a total number of three signals at δ_H6.94 (1H, dd, $J = 2.6$, 1.5 Hz, H-3), δ_H 6.85 (1H, dd, $J = 3.7$, 1.5 Hz, H-5) and δ_H 6.18 (1H, dd, $J = 3.7$, 2.5 Hz, H-4). ^{13}C NMR (CD_3OD-d_4, 126 MHz): The ^{13}C NMR spectrum showed the presence of five signals, including one carboxyl group at δ_C 164.5 (C-6), one quaternary carbon at δ_C 123.9 (C–2). DEPT135 showed only three signals with methine (CH) group at δ_C 110.6 (C–4), δ_C 116.6 (C–3) and δ_C 123.9 (C–5) (Table S1). From the NMR data, stress metabolite (SM-1) was identified as a compound pyrrole-2-carboxylic acid [22] (Figure S4-7).

Stress metabolite (SM–2)

Stress metabolite (SM–2) was isolated as a light yellow powder. The molecular formula C11H13NO3 was established by ESI–MS m/z 230 [M + Na] +. 1H NMR (CD3OD-d4, 500 MHz) showed a total number of 8 signals at δ_H 6.20 (1H, m, H-10), δ_H 6.08 (1H, dd, J = 8.9, 5.5 Hz, H-9), δ_H4.73 (1H, s, H-3), δ_H 4.69 (1H, d, J = 6.8 Hz, H-2), δ_H 4.37 (1H, d, J = 6.8 Hz, H-6), δ_H 3.58 (2H, m, H-7), δ_H 2.48 (1H, m, H-8a), and δ_H 1.88 (4H, m, H-11, H-8b). 13C NMR (CD3OD-d4, 126 MHz): The 13C NMR spectrum showed the presence of 11 signals, including three quaternary carbons at δC 160.5 (C-1), δC 144.7 (C-5), δC 139.8 (C-4). DEPT135 shows a total no of eight signals, including one methyl (CH3) group at δC 15.0 (C-11), five methine (CH) groups at δC 124.5 (C-10),

δC 119.1 (C-9), δC 83.8 (C-2), δC 75.1 (C-3), δC 60.4 (C-6), and two methylene (CH2) groups at δC 40.9 (C-7), and δC 23.5 (C-8) (Table S2). From the NMR data, stress metabolite (SM-2) was identified as a compound streptazolin [23] (Figure S8-11).

Stress metabolite (SM-3)

Stress metabolite (SM-3) was isolated as a yellowish oil. The molecular formula C_9H_7NO was established by ESI–MS *m/z* 168 [M + Na] $^+$. ^{1}H NMR (CD_3OD-d_4, 500 MHz) displayed a total number of five signals, among which there is one aldehyde matrix proton signal at *δ* 9.86 (1H, s, H-1) in the low field region and five sets of aromatic ring proton signal at δ_H 8.17 (1H, dd, J = 7.2, 1.8 Hz, H-5), δ_H 7.95 (1H, s, H-8), δ_H 7.46 (1H, m, H-3), δ_H 7.25 (2H, pd, *J* = 7.1, 1.4 Hz, H-6, H-7). According to the coupling constant and the splitting peak, it can be seen that there is an ortho-substituted benzene ring and another aromatic ring proton indole ring structure. ^{13}C NMR (CD_3OD-d_4, 126 MHz): The ^{13}C NMR presented the presence of nine signals, including three quaternary carbons at δ_C 136.9 (C-9), δ_C 123.9 (C-4), δ_C 118.2 (C-2). DEPT135 shows a total no of six signals, including one carbonyl signal at δ_C 185.5 (C-1), and five other signals at δ_C 137.5 (C-3), δ_C 123.4 (C-5), δ_C 122.0 (C-6), δ_C 120.7 (C7), and δ_C 111.5 (C-8) (Table S3). From the NMR data, stress metabolite (SM-3) was identified as a compound 3-indolcarbaldehyde [24] (Figure S12-15).

Stress metabolite (SM-4)

Stress metabolite (SM-4) was isolated as a white powder with molecular formula $C_{22}H_{20}N_4O_2$. The molecular formula $C_{22}H_{20}N_4O_2$ was established by ESI–MS *m/z* 395 [M + Na] $^+$.^{1}H NMR (500 MHz, DMSO- d_6) displayed a total no of ten signals at δ_H 10.81 (1H, d, J = 2.4 Hz, H-1), δ_H 7.70 (2H, d, J = 2.7 Hz, H-4, H-4'), δ_H 7.33 (2H, d, J = 7.9 Hz, H-7, H-7'), δ_H 7.27 (2H, dt, J = 8.1, 1.0 Hz, H-6, H-6'), δ_H 7.02 (2H, ddd, J = 8.2, 7.0, 1.2 Hz, H-5, H-5') δH 6.93 (1H, ddd, J = 8.0, 7.0, 1.1 Hz, H-13), δ_H 6.56 (2H, d, J = 2.3 Hz, H-2, H-2'), δ_H 3.85 (2H,dt, J = 6.7, 3.4 Hz, H-11, H-11'), δ_H 2.68 (1H, dd, J = 14.3, 4.2 Hz, H-10), δ_H 2.15 (1H, dd, J = 14.3, 6.7 Hz, H-10'). 13C NMR (126 MHz, DMSO-d6). The 13C NMR spectrum showed the presence of 11 signals indicating the possibility of a symmetric skeleton. DEPT showed total no seven signals, including one methylene group at δC 31.8 (C-10, C-10') and methine groups at δ_C 57.1 (C-11, C-11'), δ_C 113.1 (C-7, C-7'), δ_C 120.4 (C-4, C-4'), δ_C 120.2 (C-5, C-5'), δ_C 122.6 (C-6, C-6'), δ_C 126.2 (C-2, C-2'). The quaternary carbons were at δ_C 168.6 (C-12, C-12'), δ_C 137.9 (C-9, C-9'), δ_C 129.2 (C-8, C-8'), δ_C 110.6 (C-3, C-3') (Table S4). From the NMR data, stress metabolite (SM-4) was identified as a compound cyclo (L-trp-L-trp) [25] (Figure S16-19).

Stress metabolite (SM-5)

Stress metabolite (SM-5) was isolated as a yellow oil. The molecular formula $C_{28}H_{42}O$ was established by ESI–MS *m/z* 417 [M + Na] $^+$. ^{1}H NMR (DMSO- d_6, 700 MHz) NMR showed a total number of five signals, but according to the molecular formula, there are 42 hydrogens, indicating that the structure is highly symmetrical, and there are three groups of benzene ring proton signals at δ_H 7.44 (2H, d, *J* = 8.6 Hz, H-6, H-6'), δ_H 7.37 (2H, t, *J* = 2.0 Hz, H-3, H-3'), δ_H 7.13 (2H, dd, *J* = 8.7, 2.5 Hz, H-5, H-5'), and two sets of methyl signals at δ_H 1.32 (18H, s, H-12, H-13, H-14, H-12', H-13', H-14'), and δ_H 1.29 (18H, s, H-8, H-9, H-10, H-8', H-9', H-10'). ^{13}C NMR (DMSO-d_6, 176 MHz): The ^{13}C NMR spectrum showed the presence of ten signals, including six groups of benzene ring carbon signals at δ_C 146.7 (C-1, C-1'), δ_C 146.6 (C-2, C-2'), δ_C 137.7 (C-4, C-4'), δ_C 123.8 (C-3, C-3'), δ_C 123.4 (C-5, C-5'), δ_C 118.1 (C-6, C-6'), two groups of methine carbon signals at δ_C 34.1 (C-7, C-7'), and δ_C 33.8 (C-11, C-11'), and 2 groups of methyl carbon signals at δ_C 30.7 (C-8–10, C-8'-10') and δ_C 29.4 (C-12–14, C-12'-14') (Table S5). From the NMR data, stress metabolite (SM-5) was identified as a known compound 2, 2'-oxybis (1,4-di-tert-butylbenzene) [26], and this is the first report showing isolation of this compound from marine bacteria (Figure S20-23).

Stress metabolite (SM-6)

Stress metabolite (SM–6) was isolated as a white powder. The molecular formula $C_{14}H_{19}NO_4$ was established by ESI–MS *m/z* 288 [M + Na] $^+$. ^{1}H NMR (CD_3OD-d_4, 500 MHz): The proton NMR showed a total number of nine signals at δ_H 7.1 (2H, m, H-3'), δ_H 6.83 (2H, m, H-4'), δ_H 4.74 (1H, dd, *J* = 3.7, 1.2 Hz, H-3), δ_H 4.09 (1H, m, H-4), δ_H 3.75 (3H- d, *J* = 1.2 Hz, OCH_3), δ_H 3.49 (1H, td, *J* = 7.5, 3.7 Hz, H-2), δ_H 2.76 (2H, d, *J* = 7.5 Hz, H-5), δ_H 2.68 (2H,m, H-1'), δ_H 2.11 (3H, s, $COCH_3$). ^{13}C NMR (CD_3OD-d_4, 126 MHz). The ^{13}C NMR spectrum showed the presence of total 12 signals including two methyl at δ_C 20.9 and δ_C 55.6, two methylene at δ_C 34.9 (C-1') and δ_C 53.5 (C-5), five methine at δ_C 130.7 (C-3'), δ_C 114.9 (C-4'), δ_C 81.3 (C-3), δ_C 76.7 (C-4), δ_C 62.6 (C-2) and three quaternary carbons were present at δ_C 171.9, δ_C 159.7 (C-5') and δ_C 132.1 (C-2'), (Table S6**).** The resonances at δ_C 114.9 and δ_C 130.7 each represent two aromatic methine carbons. From the NMR data, stress metabolite (SM-6) was identified as anisomycin (Figure S24-27).

Response surface optimization for SM-6

The results of the RSM study using BBD for optimizing fermentation medium using four factors, including heavy

metal, sucrose, time, and salt, are presented here. A total of 29 experiments were conducted, and the results were analyzed to determine the optimal conditions for the best production of the SM-6. The response was measured in terms of actual factors of production. The results of experimental runs are summarized in (Table S7). The table shows that all four factors were examined deeply to investigate which factor has a high and which factor has a less influence on production. The model's suitability was expressed by the coefficient of determination (R^2) 0.8790, indicating that the model could explain 87.90% of the total variation in the response variable (HM). The adjusted coefficient R^2 was 0.7579, indicating that the model was highly significant. Furthermore, The ANOVA analysis showed that all the factors significantly affected the response variable ($p < 0.05$). The Model F-value of 7.26 implies the model is significant (Table 2). Values of "Prob > F" less than 0.0500 indicate model terms are significant and our model was highly significant (Table 2). Finally, to determine the suitability of the fitted model, the experimental and predicted values were compared. It can be seen that the run 26 production was achieved as predicted by the system (Table S7).

Factors affecting stress metabolites production

To enhance the yield of stress metabolite (SM), it is crucial to regulate the expression of factors that promote the biosynthesis of stress metabolite. Previous research has shown that metabolite production in the medium can be stimulated by various external factors, including culture time, nutrient composition such as sucrose and salt, physical stimulation like temperature and ultrasonication, and inducer supplementation with heavy metals [11]. Therefore, to enhance the production of SM, culture time maintaince, nutrient supplementation with sucrose and salt, and the addition of heavy metal ions with specific concentration as an inducer were chosen as the means to achieve this goal. Experiments were carried out to optimize the concentration of each factor that affects the production of SM, along with the culture time, through single-factor experiments. The final predictive equation obtained after neglecting the non-significant terms for is given below;

$$\begin{aligned} Y_1 = &+ 6.30 - 0.30A + 0.11B \\ &+ 0.12C - 0.21D + 0.25AB \\ &+ 0.050AC + 0.000AD - 0.32BC \\ &+ 0.15BD + 0.33CD - 1.28A^2 \\ &- 0.57B^2 - 0.46C^2 - 0.92D^2 \end{aligned}$$

The response surface contour plots were generated to visualize the effect of the four factors on SM production (Fig. 3). The response surface plot for SM production affected by culture time and sucrose is shown in Fig. 4A. As it can be seen SM production was minimal with the 4.7 mg/L at the initial culture of the seventh day with the sucrose level of 15 mg/L. But with the gradual increase of culture time, the SM production also started to increase

Table 2 Table of ANOVA analysis

Source	Sum of squares	df	Mean square	F Value	p-value Prob > F	
Model	17.25	14	1.23	7.26	0.0003	Significant
A-Time	1.08	1	1.08	6.36	0.0244	
B-Sucrose	0.14	1	0.14	0.83	0.3777	
C-salt	0.16	1	0.16	0.96	0.3432	
D-Metal	0.52	1	0.52	3.07	0.1017	
AB	0.25	1	0.25	1.47	0.2449	
AC	1.000E-002	1	1.000E-002	0.059	0.8117	
AD	−3.553E-015	1	−3.553E-015	−2.093E-014	1.0000	
BC	0.42	1	0.42	2.49	0.1369	
BD	0.090	1	0.090	0.53	0.4785	
CD	0.42	1	0.42	2.49	0.1369	
A^2	10.68	1	10.68	62.95	< 0.0001	
B^2	2.11	1	2.11	12.45	0.0033	
C^2	1.36	1	1.36	8.03	0.0133	
D^2	5.50	1	5.50	32.41	< 0.0001	
Residual	2.38	14	0.17			
Lack of fit	2.38	10	0.24			Non-significant
Pure error	0.000	4	0.000			
Cor Total	19.63	28				

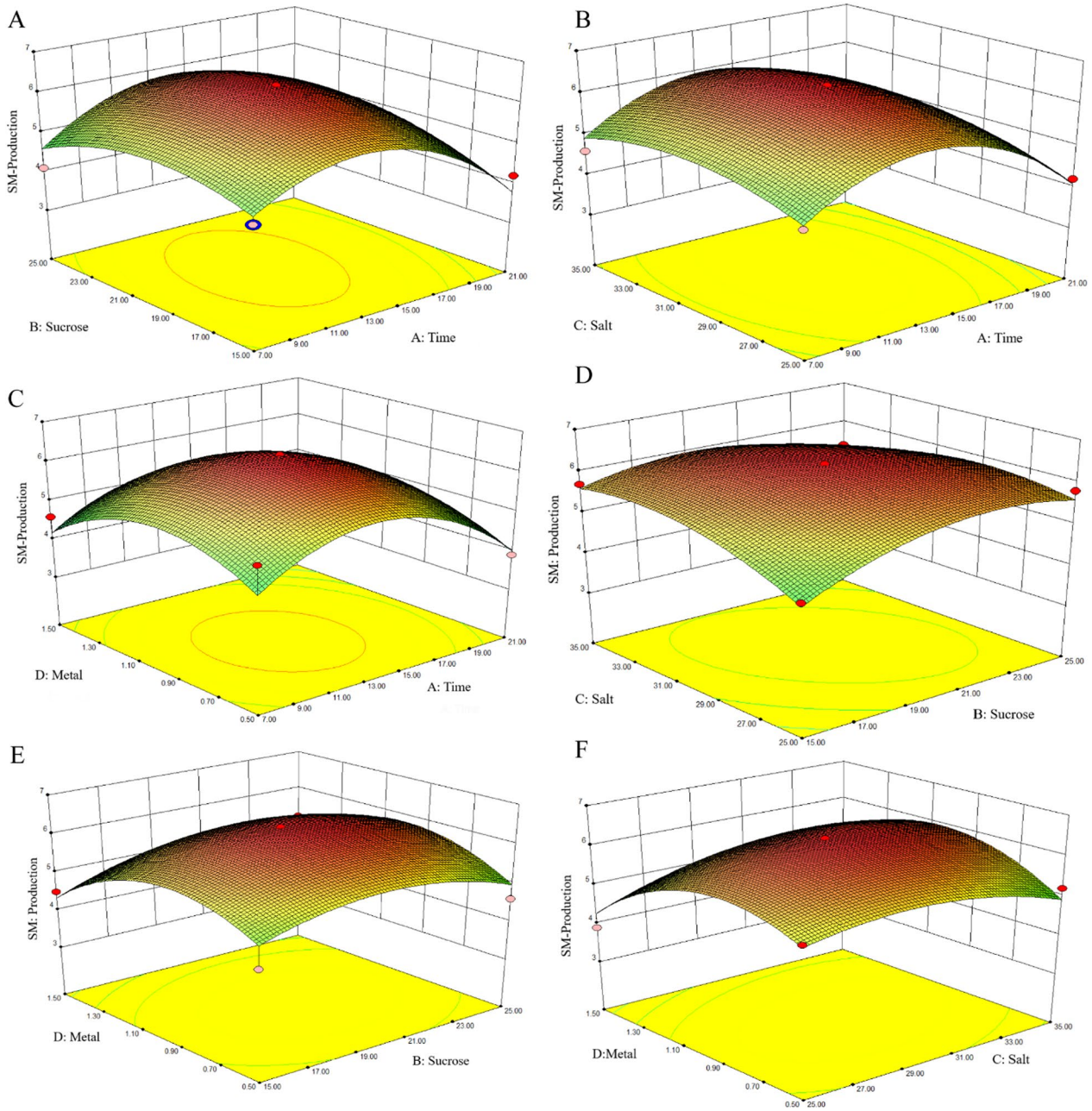

Fig. 3 Response surface graphs representing the effect of Time (**A**), Sucrose (**B**), Salt (**C**) and metal (**D**) on the responses. **A** Relative effect of Time and sucrose on SM production at constant salt and metal levels (**B**) Relative effect of Time and salt factors on SM production at constant sucrose and metal ions (**C**) Relative effect of time and metal ions on SM production while keeping sucrose and salt as a constant factor (**D**) Relative effect of sucrose and salt on SM production with time and metal ions as constant (**E**) Relative effect of sucrose and metal on SM production with time and salt as constant (**F**) Relative effect of salt and metal on SM production with time and sucrose as constant

and reached to its top on the14th day 6.3 mg/L, with the sucrose level of 20 gm/L, but after 14 days, the production started to decline gradually with the culture time. The effect of sucrose on production was also same as culture time, an increase in supplementation of sucrose elevated the level of production and reached to its top production during supplementation of 20 gm/L and with the addition of sucrose supplement to 25 gm/L declined the production of SM. During the process, the other two factors metal and salt were constant with 1 mM and 30 gm/L. Bacteria undergo four distinct stages during their life cycle. In the first stage, they initiate their growth by

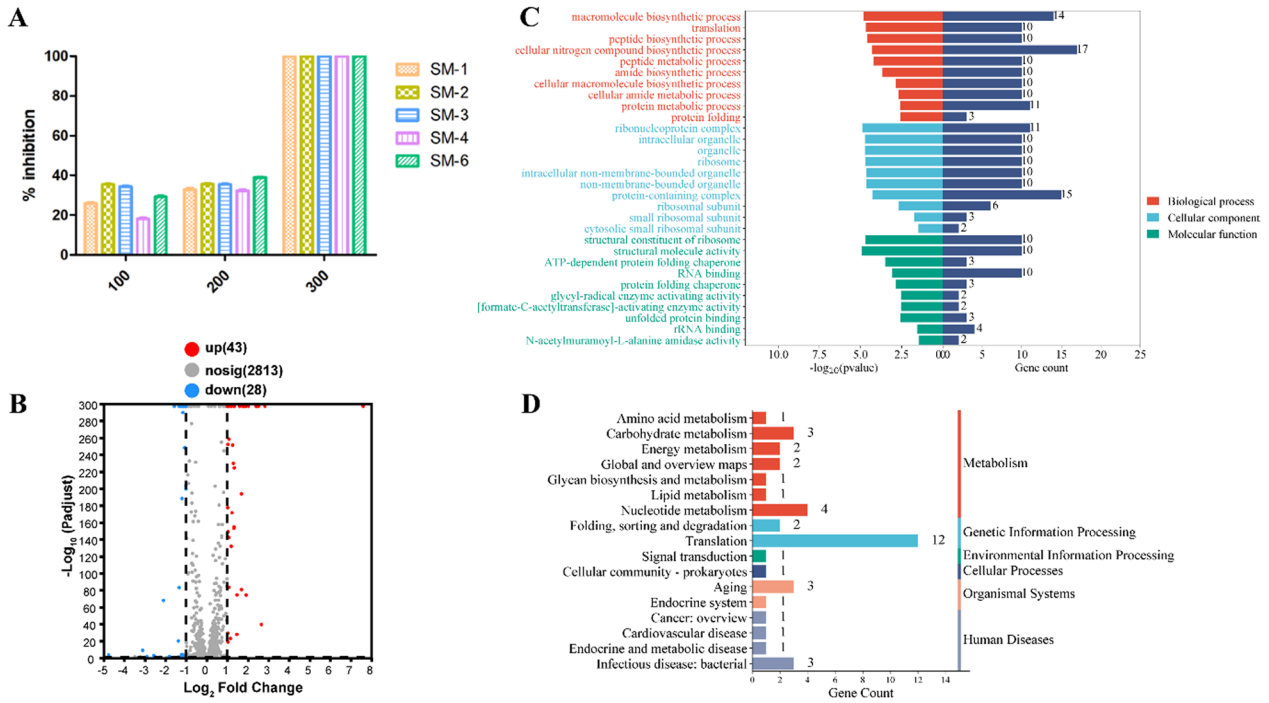

Fig. 4 Transcriptomic analysis of DEGs in SM-6 treated group. **A** Anti-bacterial activity of SM's (1–4, 6) against *S. aureus*. **B** Volcano plot of DEGs. The red dots represent up-regulated DEGs and the blue dots represent down-regulated DEGs. **C** GO enrichment analysis of DEGs. Red involves biological process processes, blue involves cellular component processes, and green involves molecular function processes. **D** KEGG enrichment analysis of DEGs

maturing and entering the second phase of life, wherein they begin to undergo cell-doubling. However, if the essential nutrients required for growth are not adequately provided, the bacteria enter the stationary phase, wherein their growth stops due to growth-limiting factors. If the nutrients continue to remain insufficient for an extended period of time, the bacteria cells begin to die. The production of SM was found to be heavily influenced by the duration of the culture period. SM production began to increase from the second day and peaked on the 14th day, during which the highest amount of SM produced. Thereafter, the production of SM began to decline from the 15th day onwards (Fig. 3A–C).

The response surface plot for SM production affected by culture time and salt is showed in Fig. 5B. The SM production reached to its top with the supplementation of sea salt at 30 gm/L. The response surface plot for SM production affected by culture time and heavy metal (Nickel) is showed in Fig. 3C. The SM production reached to its top with the supplementation of nickel 1 mM ions. But as it can be seen that metal and culture time have a great influence on SM-production, a little increase or decrease in heavy metal concentration declined the production. Figure 3D, from the contor plot it can be senn that both nutrient supplementation salt and sucrose dosent have that much negative affect on SM production. While Fig. 3E and F here by showed that sucrose:metal and salt:metal both have affect on declining SM- production. From over all results it can be seen that a little fluctuation in nickel ions concentration cause a big affect on SM-production. The presence of metal ions in the culture medium can influence the synthesis of secondary metabolites and may alter aspects of secondary metabolism, resulting in changes in the production of bioactive compounds. Studies have shown that metals such as copper, cobalt, nickel, zinc, silver, and iron can induce the production of secondary metabolites in various microorganisms [5, 27].

The production of SM was found to be affected by the concentration of nickel ions present in the fermentation medium. The highest enhancement in SM production was observed when the metal ion concentration was 1 mM. However, initial and high concentrations of metal ions resulted in decreased SM production. These results suggest that heavy metals can effectively stimulate the cryptic secondary metabolism of microorganisms.

Finally the optimum values for SM production was achieved with culture time 14 days, 20 gm/L sucrose, 30 gm/L salt, and 1 mM nickel ions resulted in production of SM with 6.3 mg/L. These results demonstrate that the

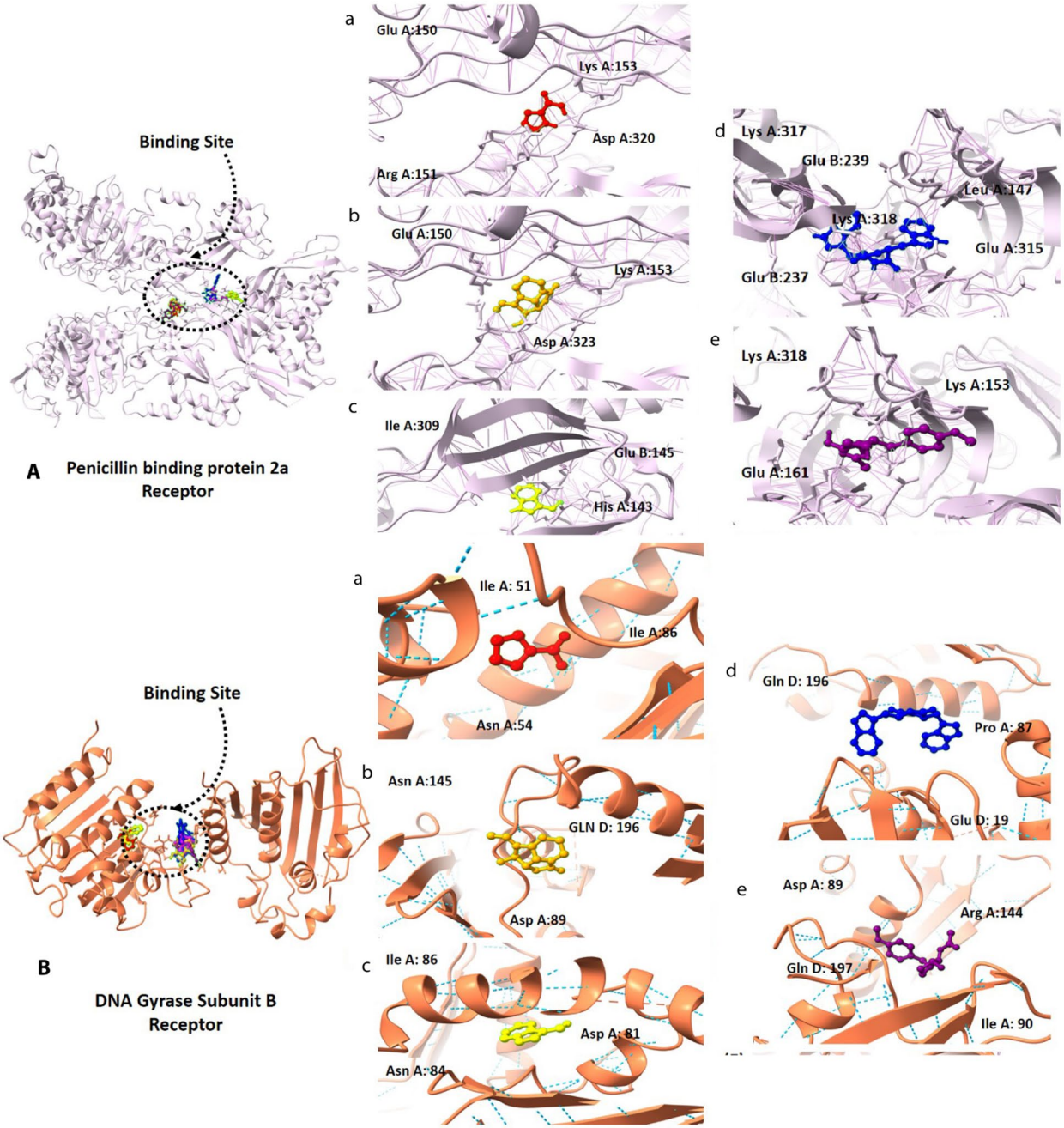

Fig. 5 **A**. 3D figures of molecular docking analysis with target Penicillin binding protein 2a. (**a**)1 (**b**) 2 (**c**) 3 (**d**) 4 (**e**) 6. **B** 3D figures of molecular docking analysis with target DNA Gyrase Subunit B. (**a**) 1 (**b**) 2 (**c**) 3 (**d**) 4 (**e**) 6

predictions made using response surface methodology were accurate and reliable. The use of the Box-Behnken statistical design was effective in determining the optimal conditions for SM production, indicating that this method is a powerful tool for optimizing biotechnological processes. Overall, these findings highlight the importance of using statistical techniques to optimize production processes and improve efficiency.

Transcriptomic analysis unveiling antimicrobial mechanisms

Screening for antimicrobial activity

The antibacterial activity of all stress metabolites was initially tested against ten pathogenic microbes but only 5 stress metabolites (1–4, 6) showed interesting results against *S. aureus,* while SM-5 did not show good activity against any pathogenic bacteria. Stress metabolites

1–4, and 6 were re-evaluated against *S. aureus* at three different concentrations of 100, 200 and 300 μM. All compounds showed weak inhibition at 100 μM, moderate inhibition at 200 μM and 100% inhibition at 300 μM (Fig. 4A). The survival of bacteria measured as OD-600 on a microplate reader, showed that all compounds are bactericidal at 300 μM. The results showed that heavy metals triggered compounds could be potentially investigated for anti-microbial activity.

Differentially expressed genes (DEGs)

The preceding investigations provided compelling evidence for the remarkable antibacterial efficacy exhibited by the SM-6 against *S. aureus*, and transcriptomic analysis was performed to gain deeper insights into the underlying mechanism. The RNA samples obtained from SM-6 treatment group and the control group were of high quality following the filtration of raw sequencing data, and the resulting sequencing data exhibited a Q30 trimming percentage of 94%, surpassing the threshold of 90% (Table S8). Furthermore, a total of 71 DEGs were identified, with 43 genes up-regulated and 28 genes down-regulated (Fig. 4B), with detailed information of DEGs described in Table S9-S10.

Functional annotation analysis of DEGs

The DEGs were subjected to annotation and enrichment analysis utilizing the Gene Ontology (GO) database, a globally recognized system for classifying gene functions into three categories: biological process (BP), cellular component (CC), and molecular function (MF). The results of the GO classifications and functional enrichment analysis for the DEGs are presented in Fig. 4C. The results of Gene Ontology (GO) analysis indicate that, following treatment with the SM-6 compound, a majority of differentially expressed genes (DEGs) within the Biological Process (BP) category are associated with the biosynthetic processes of macromolecules. The primary impact is observed in the biosynthesis of large biomolecules, notably proteins. Specifically, these DEGs significantly participated in various biological processes related to proteins, including peptide biosynthetic process, translation, protein folding, as well as the metabolism of peptides and proteins. In terms of CC, the most prominent enrichment of DEGs was located in ribosomes, ribonucleoprotein complexes, and ribosomal subunits. Moreover, considerable enrichment of DEGs involving in organelle parts, cellular parts, and ribosome composition were observed. Regarding MF, it has been observed that DESs participates in influencing the structural components of ribosomes, ATP-dependent protein folding chaperone, and the binding of rRNA and RNA. This suggests that the structural integrity and functional dynamics of *S. aureus* ribosomes may be compromised, inhibiting the biological functions of proteins.

KEGG enrichment analysis was conducted to comprehensively investigate the functional roles of the DEGs, aiming to classify the DEGs into distinct pathways by utilizing bioinformatic databases. Multiple upregulated pathways closely associated with antibacterial processes were discovered, revealing the underlying mechanism of *S. aureus* cells with the treatment of SM-6 (Fig. 4D). In the Bacterial Genetic Information Processing pathway category, the highest number of DEGs (gene count: 12) were significantly enriched in the translation process, and two DEGs were enriched in the folding process, indicating that the compound SM-6 exerted its antimicrobial effect by inhibiting the translation and folding processes of proteins in *S. aureus* cells. Furthermore, within the Metabolism pathway category, we observed enrichments in nucleotide, carbohydrate, and energy metabolism processes, with 4, 3, and 2 DEGs respectively. This implied that SM-6 may exert its antimicrobial effects by actively participating in and modulating various metabolic processes within bacterial cells. These findings contribute to a more comprehensive understanding of the molecular mechanisms underlying the antimicrobial actions of the compound 6.

Core DEGs related to protein folding and protein synthesis

DnaK and groEL were genes encoding heat shock proteins, playing crucial roles as molecular chaperones and a chaperone system within cells, aiding in maintaining the correct structure and functionality of proteins in response to environmental stress [28]. These chaperones interact with newly synthesized proteins, facilitating their correct folding into functional structures. Additionally, they can unfold and refold denatured proteins, aiding in the restoration of their activity. DnaK and groEL genes also contribute to cellular stress response, particularly under conditions such as high temperature and oxidative stress. Their expression can be upregulated to assist cells in coping with adverse environmental conditions. Overall, DnaK and groEL play a crucial role in maintaining protein stability and functionality, essential for ensuring normal cell survival and adaptability. In our study, as presented in Table S9, revealed a significant down-regulation of the dnaK and groEL genes in *S. aureus* cells upon the addition of the SM-6 compound. This phenomenon suggested that SM-6 may directly impact the protein synthesis process in *S. aureus* cells, reducing the need for abundant molecular chaperone proteins like dnaK and groEL to assist in proper folding. This could be attributed to the direct action of compound 6 on the protein synthesis machinery, resulting in decreased reliance on

molecular chaperones. On the other hand, SM-6 may exert a toxic effect on bacteria, leading to the downregulation of dnaK and groEL genes as a survival strategy in response to the drug-induced cellular damage. Bacteria may adjust their metabolism and survival strategies by decreasing the expression of heat shock proteins to adapt to the cellular injury caused by the drug.

On the other hand, the ribosome, as a crucial stage in protein synthesis, orchestrates the dynamic process of translation and serves as the site for protein biosynthesis in all cells, representing a primary target affected by compound 6 in *S. aureus* bacteria. The bacterial ribosome comprises a large 50S subunit and a small 30S subunit, forming a 70S ribonucleoprotein complex responsible for converting mRNA into corresponding polypeptide chains. The 50S subunit of the ribosome contains 23S and 5S rRNA, engaging with aminoacyl-tRNA to catalyze peptide transfer and regulate the elongation process, while the 30S subunit contains 16S rRNA, interacting with mRNA to initiate protein synthesis. Protein synthesis involves four major steps: initiation, elongation, termination, and recycling, with the first two steps being common targets of numerous antibacterial agents [29]. In our investigation, significant upregulation was observed in genes encoding 30S ribosomal proteins (rpsD, rpsO, rpsI, and rpsF) and 50S ribosomal proteins (rplM, rplS, rplU, rpmH, and rpmI) upon exposure to SM-6, as indicated in Table S10. This suggested that SM-6 may target the ribosome of *S. aureus* bacteria, disrupting protein synthesis steps and triggering a response in the *rps* and *rpm* gene families. Bacteria might attempt to counteract SM-6-induced ribosomal damage by enhancing the expression of these gene families. Additionally, SM-6 induced oxidative stress in the cellular environment of *S. aureus*. In response, bacteria upregulate the *rps* and *rpm* gene families to cope with this cellular stress, ensuring the maintenance of normal cellular survival and function. Simultaneously, the significant upregulation of the spxA gene, encoding the spxA protein, in Table S10 underscored the disruption of the oxidative-reductive balance within *S. aureus* cells, confirming that compound 6 elicited oxidative stress responses, leading to oxidative damage and inhibition of bacterial growth [30]. In summary, compound 6 modulated the expression of heat shock protein genes dnaK and groEL, influencing the cellular protein folding mechanism. Additionally, it interfered with protein synthesis at the ribosomal level, disrupts the cellular redox balance, and consequently comprehensively inhibited the normal growth of *S. aureus*.

Pharmacokinetic and toxicological properties

Absorption, distribution, metabolism, excretion, and toxicity (ADMET) prediction studies were conducted for the stress metabolites (SM-1-4, 6).

Pharmacokinetic properties

The physicochemical properties of the stress metabolites SMs 1–4, and 6 are given in Table 3. The physicochemical properties were analyzed based on 6 major parameters to indicate oral bioavailability (Table 3). The topological polar surface area (TPSA) scores of all SMs were in the range of 20Å^2 to 130Å^2, suggesting the SMs (14, 6) having good transport properties in vivo. Figure S28 displays the oral bioavailability of the SMs. The SMs (14, 6) showed that the results were within these limits, except 3 and 4 were out of domain for insaturation, indicating that SMs 14, and 6 have good physiochemical profiles. Among all the compounds, the best results were observed for compound 6.

ADMET

HIA and CNS absorption serve as crucial parameters assessed for every biomolecule prior to its consideration for drug formulation in pharmaceutical or clinical trials [31]. Blood–brain barrier (BBB) penetration is particularly important, as compounds targeting the central nervous system (CNS) must traverse the BBB, while those intended to remain inactive within the CNS should not cross it to prevent potential adverse effects [32]. As indicated in Table 3, SM-4 exhibits high gastrointestinal absorption (HIA) with minimal BBB permeability. The BOILED-EGG graph (Figure S29) provides predictions for GI absorption (HIA) and BBB penetration of all SMs (1–4, 6) [33].

Moreover, this tool also provides predictions for five major cytochrome (CYP) isoforms. These enzymes are pivotal in drug metabolism, collectively metabolizing approximately 75% of drugs available in the market. Inhibition of any of these isoforms can lead to significant pharmacokinetic-based drug-drug interactions [34]. As indicated in Table 3, SMs 1, 2, and 6 demonstrate no inhibition of any cytochrome isoforms and exhibit rapid metabolism, indicating their unlikely involvement in drug-drug interactions mediated by these specific cytochromes. While, compound 3 inhibited one cytochrome CYP1A2 but compound 4 inhibited 4 cytochromes and can cause drug-drug interaction.

In the context of excretion, drug clearance is determined by combining hepatic and renal clearances, a critical factor in determining dosing rates to achieve steady-state concentrations. However, all SM exhibited low clearance values, non-hepatotoxic, and were within the safe domain range.

Table 3 Predicted physicochemical parameters and ADMET properties of SMs (1–4, 6)

Properties	Parameters	1	2	3	4	6
Physicochemical properties	MW[a] (g/mol)	111.10	207.23	145.16	372.42	265.30
	Rotatable bonds	1	0	1	4	5
	HBA[b]	2	3	1	2	5
	HBD[c]	2	1	1	4	2
	Fraction Csp3	0.00	0.55	0.00	0.18	0.50
	TPSA[d]	53.09	43.77	32.86	89.78	67.79
Lipophilicity Log $P_{o/w}$	iLOGP	0.70	1.79	1.12	1.91	2.34
	XLOGP3	0.85	−0.20	1.93	2.93	0.90
	MLOGP	−0.36	0.95	0.88	1.43	0.71
Absorption	Water solubility (mol/L)	−2.059	−2.457	−1.948	−3.212	−1.417
	Caco2 permeability (10^{-6} cm/s)	1.127	1.2	1.622	0.88	0.471
	Intestinal absorption (human) (% absorbed)	88.64	86.19	93.376	94.30	74.969
	Skin permeability (log/kp)	−2.735	−3.803	−2.352	−2.736	−2.824
	P-glycoprotein substrate	No	No	No	Yes	No
Distribution	VDs (human)	−1.027	0.243	0.02	−0.011	0.391
	BBB permeability (log BB)	−0.389	−0.158	0.413	−0.596	−0.24
	CNS permeability (log PS)	−2.946	−2.996	−1.666	−2.301	−2.871
Metabolism	CYP1A2 inhibitor	No	No	Yes	Yes	No
	CYP2C19 inhibitor	No	No	No	Yes	No
	CYP2C9 inhibitor	No	No	No	Yes	No
	CYP2D6 inhibitor	No	No	No	No	No
	CYP3A4 inhibitor	No	No	No	Yes	No
Excretion	Total clearance (log ml/min/kg)	0.662	0.441	0.449	0.734	0.956
	Renal OCT2 substrate	No	No	Yes	No	No
Toxicity	Max tolerated dose (log /mg/kg/day)	0.778	0.673	0.397	0.198	-0–115
	hERG I inhibitor	No	No	No	No	No
	hERG II inhibitor	No	No	No	Yes	No
	Oral Rat Acute toxicity LD50, (mol/kg)	2.206	1.975	2.307	2.763	2.681
	Hepatotoxicity	No	No	No	No	No
	Skin sensatisation	No	No	Yes	No	No
	T. Pyriforms toxicity (log ug/L)	0.247	0.168	0.255	0.297	0.269
	Minnow toxicity (log mM)	2.812	1.95	0.716	1.275	1.471

[a] Molecular weight, [b]H-bond acceptor, [c]H-bond donor, [d]Topological polar surface area

Cardiac toxicity

The blockade of hERG K+channels has been associated with the occurrence of fatal cardiac arrhythmias, prompting the FDA to mandate hERG safety assessments for any biomolecule under consideration as a drug candidate. Figure S30 depicts the probability map of SMs (1–4, 6) derived from cardiac toxicity predictions by pred-hERG. This map illustrates the positive and negative contributions of atoms or fragments to hERG blockage, with intense pink color indicating a negative contribution. According to pred-hERG predictions, SM-1 was identified as non-cardiotoxic with a 90% confidence value, SM-2 as non-cardiotoxic with a 70% confidence value, SM-3 and SM-4 as potential cardiotoxic with a 60% confidence value, and SM-6 as non-cardiotoxic with a 50% confidence value. These results suggest that SM-1, SM-2, and SM-6 are safer options in terms of cardiac safety.

Molecular docking

Ligand and protein preparation

The in-vitro antibacterial assays indicatedthat all SMs 14, and 6 showed activity against *S. aureus.* So initially we have targeted two proteins for each pathogen. The proteins selected for *S.aureus* based on literature search were obtained from PDB as DNA GYRASE SUBUNIT B (pdb id: 4uro) and Penicillin binding protein 2a (PBP2a)

(pdb id: 1mwt). All the SMs (14, 6) were prepared in SDF format using ChemBio Draw.

Ligand–protein docking

Through systematic analysis, two protein targets of *S. aureus* were selected for molecular docking. The structural refinement process utilized the UCSF Chimera tool, incorporating energy minimization with 1000 descent steps. Additionally, non-standard residues were removed from the protein receptors to prevent clashes and ensure correct configurations. Molecular docking was conducted to identify potential targets, revealing strong binding affinities between the constituents and the binding pockets of two target proteins. Docking scores, alongside binding energy values, served as primary criteria for subsequent molecular dynamics simulations (Table 4; Fig. 5). The SMs 14, and 6 have shown best binding towards both selected target proteins but the highest binding was achieved against Penicillin binding protein 2a. The interacting residues for all SMs (14, 6) against penicillin binding protein 2a, and DNA GYRASE SUBUNIT B in molecular docking analysis 3D figures are demonstrated in Fig. 5. Each of the SMs (1–4, 6) exhibited interactions with the receptor proteins, including hydrogen bonds, Pi–pi-stacked interactions, and van der Waals interactions, which are depicted by dotted lines. Additionally, the presence of hydrogen bond interactions with receptor proteins is specifically highlighted in Fig. 5.

In Fig. 5A and Figure S31 which showed the complex with Penicillin binding protein 2a (PBP2a), SM-1 was observed to bind with one hydrogen bond at GLU A: 150, while SM-2 binds with two hydrogen bonds at LYS A: 153 and ASP A: 323.While SM-3 did not show any binding with conventional hydrogen bond, compound 4 showed the best hydrogen bond among all metabolites and binds with 4 hydrogen bonds at LYS A: 317, LYS: 318, GLU B: 237 and GLU B: 239. The compound 6 binds with one hydrogen bond at LYS A: 318 and the binding energy was −10.14 with RMSD value of 1.23. The compound 6 showed the highest binding score of −10.14 against Penicillin binding protein 2a. In Fig. 5B and Figure S32, all the SMs (1–4, 6) also showed good binding against DNA GYRASE SUBUNIT B. The SMs 1–3 bind with one hydrogen bond at ILE A:51, ASN A:145, and ASP A:81, while SM-4 binds with two hydrogen bonds at GLU D:193 and GLN D: 196. The compound 6 binds with two hydrogen bonds at GLN D:197 and ARG A:144. The complex binding energy was calculated as −9.57 and the RMSD value was 2.13. Among all metabolites, compound 6 showed the highest binding score of −9.57 (Table 4). In summary, these discoveries contribute to an emerging body of evidence indicating that these two proteins may serve as promising targets for antibacterial therapy. Furthermore, more investigations are needed in exploring the binding sites of active compounds within the core protein, warranting further study.

Table 4 Molecular docking analysis of SM's (1–4, 6) against *S. aureus*

Compounds	Docking Score	Rmsd	Distances	Residues
DNA GYRASE SUBUNIT B (pdb id: 4uro)				
SM-1	−6.79	0.61	4.08	Ile A: 51 Ile A:86 Asn A:54
SM-2	−7.39	1.12	5.13 4.80 3.29	Asn A:145 GLN D: 196 Asp A:89
SM-3	−6.87	1.25	4.09	Ile A: 86 Asp A: 81 Asn A: 84
SM-4	−8.55	2.33	5.6	Gln D: 196 Pro A: 87 Glu D: 193
SM-6	−9.57	2.13	3.72 4.08 3.85 4.96	Asp A: 89 Arg A:144 Gln D: 197 Ile A: 90
Penicillin binding protein 2a (pdb id:1mwt)				
SM-1	−8.56	1.73	4.24 4.18 5.80 7.08	Glu A:150 Lys A:153 Asp A:320 Arg A:151
SM-2	−8.36	0.45	4.28 3.33 3.91	Glu A:150 Lys A:153 Asp A:323
SM-3	−6.71	0.84	4.70 5.24 4.08 3.97	Ile A:309 Glu B:145 His A:143 Asn B:146
SM-4	−9.43	1.73	2.74 5.15 4.37 3.58 5.44 4.67	Lys A:317 Glu B:239 Leu A:147 Lys A:318 Glu A:315 Glu B:237
SM-6	−10.14	1.23	6.52 6.48 5.68	Lys A:318 Lys A:153 Glu A:161

After performing molecular docking analysis, the DNA gyrase subunit B and penicillin-binding protein 2a were further docked with ciprofloxacin as a control. Ciprofloxacin is a widely-used antibiotic known for its efficacy in controlling infections associated with opportunistic human pathogens. The docking results indicated that ciprofloxacin has a binding affinity of 6.01 kcal/mol and an RMSD of 2.39 Å with DNA gyrase subunit B. In contrast, it showed a binding affinity of 5.899 kcal/mol and an RMSD of 1.82 Å with penicillin-binding protein 2a. These findings suggest that

compared to ciprofloxacin, the compounds analyzed in this study have a higher binding affinity, indicating the potentials to be more effective as therapeutic agents.

Ligand–protein docking

The docking scores and their implications for drug design are crucial in understanding how effectively a drug interacts with its target. In our study, the simulations and analysis of the ligand and three innate immune receptors, including TLR4, using HADDOCK 2.0 and PDBsum, revealed significant insights. The docking score for the TLR4-PBP2A complex is -15.6 ± 16.2 kcal/mol, indicating a strong binding affinity. This low binding energy suggests that it binds very tightly to the TLR4 receptor. Such a strong interaction is essential for ensuring that it remains effectively bound to the receptor, which is critical for its functionality. A stable binding interaction typically correlates with a drug's effectiveness, as it means the ligand can persist in its intended state within the biological environment, enhancing the likelihood of an effective immune response.The significant number of well-defined molecular interactions between the PBP2A and the TLR4 receptor further supports the stability of the docked complex. These interactions include hydrogen bonds, hydrophobic interactions, and van der Waals forces, which contribute to the overall binding affinity and stability. Understanding these specific interactions is important for drug design because it allows to pinpoint which parts of the PBP2A are crucial for its interaction with TLR4. These modifications to the PBP2A improve its binding properties and reduce potential side effects. Moreover, the interface statistics depicted in Fig. 6a provide detailed insights into how the PBP2A interacts with TLR4. By analyzing these statistics, our findings assist in better understanding of the quality of the binding interface, including the nature and number of occurred interactions.

In silico cloning within S. aureus system

To ensure the expression of proteins generated used *S. aureus* hosts, in silico cloning was carried out. First, the PBP2A was altered to use the *S. aureus* expression system codons. The optimized targets, comprising of 828 nucleotides, displayed a CAI value of 1.0 within the optimal range of 0.8–1.0, along with a GC content falling within the favorable range of 53.2% (30–70%). These characteristics suggest a high potential for reliability and favorable protein expression. The next step involved attaching the buffer-compatible BamHI and HindIII restriction sites to both ends of the optimized nucleotide sequence to aid in the purification and cloning procedure. The improved sequence was then cloned to the several cloning sites of the pET30a (+)-Tev and pCC1 vector between the restriction sites. The clone was 7.50 and 1.1 kb long as mentioned in the Fig. 6b.

Molecular dynamics simulations (MDS) and Control

MDS for ligand–protein

Control was chosen against each protein. Docking was done to cross verify the efficacy of the control compounds showed much lower results compared to the test compounds. Binding affinity for both controls are reported as −4.72, −3.81 and RMSD value of 2.8 and 3.2. The 3D and 2D interactions of proteins along with the control were indicated in the Fig. 7(A–D).

The best score complex was further analyzed for its MDs based on the docking score. The SM-6 (Penicillin

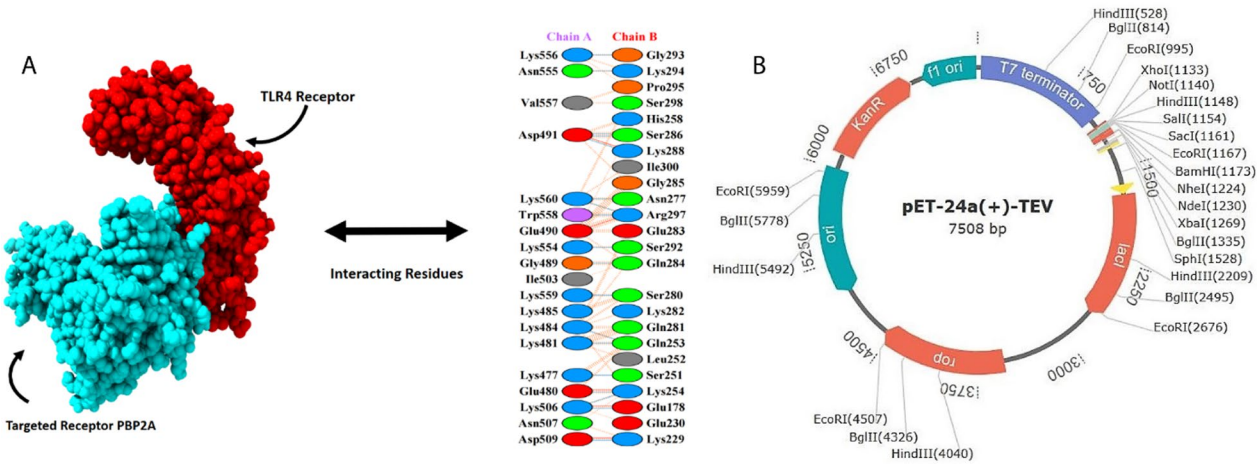

Fig. 6 **A** Docked complex of TLR4- PBP2A along interactions **B** In silico cloning of codon optimized PBP2A into *S. aureus* expression system. The plasmid back-bone is kept in black color while the inserted DNA sequence is shown

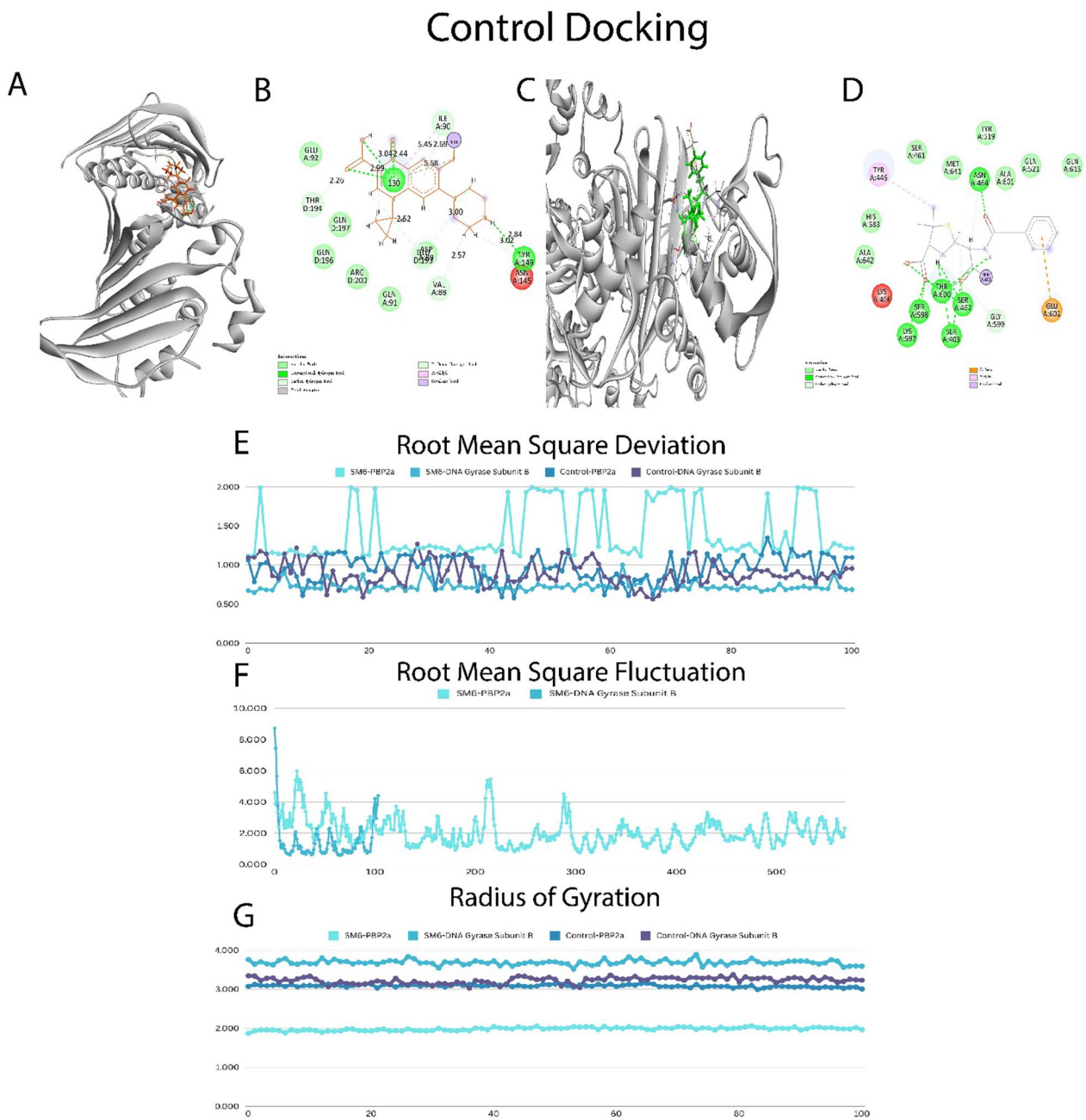

Fig. 7 (**A**–**B**) Control Docking of PBP2a representing 2D and 3D (**C**–**D**) Control Docking of DNA GYRASE SUBUNIT B representing 2D and 3D (**E**) RMSD plot of SM-6 and control with PBP2a and DNA GYRASE SUBUNIT B (**F**) RMSD plot of SM-6 with PBP2a and DNA GYRASE SUBUNIT B (**G**) RoG plot of SM-6 and control with PBP2a and DNA GYRASE SUBUNIT B

binding protein 2a) MDs were performed for 100 ns. The parameters explored for analyses such as RMSD, RMSF, protein–ligand contact, RoG, and SASA. The RMSD analysis served as a tool to assess the stability of the simulation outcomes. Throughout the simulation, the RMSD graph of the protein (left Y-axis) offers insights into its structural conformation, while the RMSD graph of the ligand (right Y-axis) indicates the stability of the ligand relative to a particular protein and its binding pocket (Fig. 7a). The compound 6 (PBP2a) complex was also stable but were with a little bit fluctuations from 25 ns till 50 ns with the fluctuation range of 2.0 Å, but after 58 ns, the system was totally stable till end (Fig. 7A). The result here by demonstrated that

the complex was stable and ligand binding to the protein's active binding region throughout the simulation tenure, which here by shows that this compound has strong affinity towards the PBP2a.

Furthermore, the ligand properties of SM-6 with PBP2a are also analyzed. In the complex of SM-6 with PBP2a, the RMSD and RoG, little bit fluctuated in the beginning till 15 ns, but after that was totally stable till 100 ns. In this complex there was no intra-hydrogen bond. The ligand's molecular surface area (MoLSA) was unstable in the start and showed little bit fluctuations till 25 ns, with in the range of 366–372, but later, it was totally stable till end. The solvent-accessible surface area (SASA) and polar surface area (PSA) also fluctuated little after 40 ns, but then stabilized till 100 ns (Fig. 7B). Protein–ligand contacts were also evaluated through MD simulations. The interactions can be categorized into four types including Hydrogen bonds (green), hydrophobic bonds (purple), Ionic bonds (pink) and water bridges (blue) figure S33.

MDS for protein–protein analysis

The MDS for protein–protein analysis was assessed using the publicly available online server IModS, renowned for its structural analysis capabilities involving adjustments to the complex's force field at various time intervals. This approach typically yields models with minimal distortion across all represented residue capacities. Eigenvalue calculations revealed a value of 4.646326e-06 for the TLR4-PBP2A complex. Low RMSD values and highly correlated regions in the heat maps indicated effective interactions among individual residues. A detailed depiction of the results from the IModS molecular dynamics simulations is provided in Fig. 8.

Discussion

This research focused on isolating metal-triggered secondary metabolites from two marine soil-oriented bacteria species. Furthermore, evaluating the bacterial species' potential to resist different kinds of metals with various concentrations. The SM's (16) were evaluated for their antibacterial activity against gram positive and gram negative bacteria through *in-vitro* assays. In-silico studies of

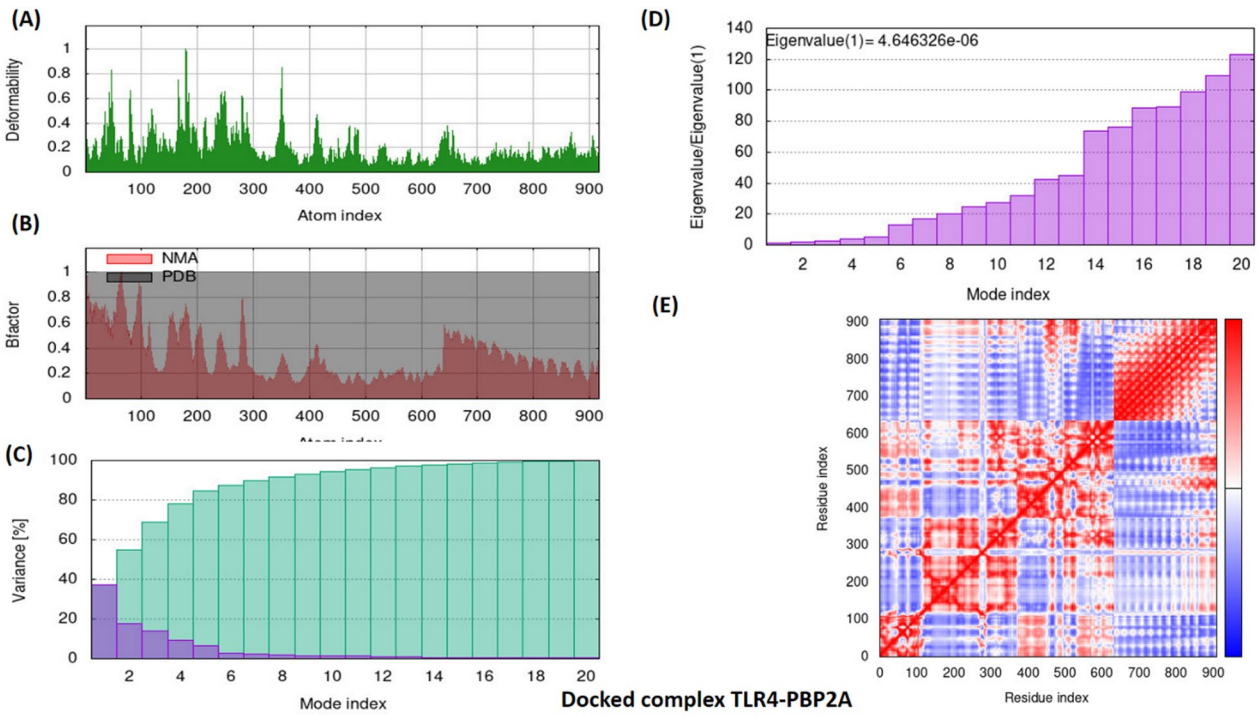

Fig. 8 The iMOD server's normal mode analysis (NMA) outputted the following plots: (**A**) Deformation Plot, illustrating regions of significant structural flexibility, with values ranging from 0 to 0.4; (**B**) B-factor, representing atomic displacement parameters to indicate the dynamic behavior of atoms; (**C**) Variance plot, displaying the variance in atomic positions to highlight flexibility within the structure; (**D**) Eigenvalues, with a specific value of 4.646326e-06, reflecting the vibrational frequency and energy of the mode; (**E**) Covariance matrix plot, visualizing the correlated movements of atoms, with anticorrelated, uncorrelated, and correlated states of atomic motion represented by the blue, white, and red hues, respectively

ADMET, molecular docking and MD simulations were also performed for the active metabolites.

Heavy metals-triggering techniques represent an emerging strategy to enhance the likelihood of producing novel secondary metabolites [35]. As evidenced by our prior investigations, compounds induced by metals are typically absent in standard culture conditions, but become apparent following the imposition of abiotic stress, such as exposure to heavy metals. Microorganisms may exhibit varying degrees of resistance or sensitivity to metals, necessitating adjustments in metal concentrations or the use of metal combinations to activate dormant genetic pathways [11, 36, 37]. Heavy metals can have both positive and negative effects on compound production, depending on the context. If the heavy metals like zinc and copper, given in certain amounts, are essential for microbial growth and metabolism. They can act as cofactors for enzymes involved in the synthesis of antibiotics or other drugs [38]. In certain microorganisms, the presence of heavy metals can trigger the production of antibiotics. This may be a defensive mechanism where the microbes produce antibiotics to compete with other organisms in metal-rich environments [39]. Some microorganisms used for bioremediation of heavy metals also produce antibiotics. The dual role of these microbes can be leveraged for both environmental cleanup and antibiotic production [40]. However, the impacts of heavy metals can be complex, and their benefits need to be carefully managed to avoid toxicity and environmental harm. Wu et all have derived two novel compounds from marine fungus by using zinc as elicitor [38]. Shi et al. has derived one novel antibiotic from marine actinomycete by using nickel as elicitor [41]. Akhter et al. has produced two antibiotics from marine actinomycete by using nickel as the main elicitor [42]. Hassan et al. [5, 43] have derived two potent compounds as anticancer, anti-inflammatory, and antioxidant agents from marine actinobacteria by using nickel, copper and zinc. Our research indicates that proteobacteria and actinobacteria strains initially did not exhibit significant responses to various metals at different concentrations. However, upon the addition of specific concentrations of nickel and zinc ions, the bacteria responded to these metal ions in their environment, producing new metabolite peaks indicative of stress responses.

Anti-bacterial agents derived from natural products have gained considerable attention as potential therapeutic agents against emerging resistant bacterial strains [44]. Plants, fungi, and bacteria themselves produce a variety of compounds that have demonstrated activity against bacterial pathogens[45]. Marine natural products can be used in the development of novel anti-infective drugs, as they offer diverse structural scaffolds with unique mechanisms of action that can overcome resistance mechanisms employed by bacteria [46, 47]. From the discovery of *Penicillin* till the journey of vancomycin and other potent antibiotics, the direction of researchers toward microorganisms is still at its peak to untap more novel interesting bioactive compounds. Additionally, natural products tend to have fewer side effects than synthetic drugs and are more readily biodegradable. In this research, we have evaluated the anti-microbial potential of stress metabolites against multiple pathogens. Heavy metals-derived compounds are proven to have potent bioactivities as anticancer [38], anti-oxidant [43], anti-inflammatory [5] and antibacterial [41, 42]. In our studies, the SM's (14, 6) have shown the best antimicrobial activity against *S. aureus.* All the SM's (1–4, 6) have achieved its IC_{50} value at 300 µM against *S. aureus* which here by proved that all these stress metabolites are very active against *S. aureus*.

Response surface methodology is one of the techniques to evaluate the multi-factors affecting on factor X [8]. In our study, we have evaluated the production of the SM-6 through box-behnken method by evaluating the four factors including culture time, heavy metal, sucrose and salt concentration affecting stress metabolite production. The ANOVA analysis has shown that the model was very significant with the p-value of 0.0003, and the SM-6 production was enhanced with the optimized condition consisting of nickel 1 mM ions, 20 mg sucrose, 30 mg salt and culture time 14 days. During this condition, the temperature was kept constant at 28 °C. Under these conditions the SM-6 production was enhanced with a value of 6.3 mg/L, which was totally absent at the normal culture of strain C2-73 and much higher than other tested metal-stress conditions.

Identifying differentially expressed genes offers new insights into the molecular mechanisms and pathways involved, paving the way for further functional studies and potential therapeutic targets [45]. In our studies, our transcriptome analysis has provided a comprehensive overview of gene expression changes under varying conditions, highlighting the dynamic regulatory networks that underpin cellular responses. Further in-depth evaluation of molecular docking and simulation of antibacterial activity has been performed for pathogenic bacteria. Two proteins for bacteria have been selected for docking against all stress metabolites, and all the SM's (14, 6) have shown the best docking score against Penicillin-binding protein 2a for *S. aureus.* Further MDS have also proved that compound 6 has good binding activity and has shown stability inside the protein core of the targeted proteins. However, despite the potential benefits of natural products, their efficacy and safety require further

exploration before they can be fully integrated into the arsenal of antimicrobial agents.

Chemoinformatics is one of the new and fastest tools for drug discovery by using algorithms. In this technique less time is required to search for libraries of compounds for specific kinds of diseases and this tool made it easy for a single compound to investigate it for multiple diseases. It is a must for every compound to be investigated for its ADMET and other tests before it enters into clinical trials. Thanks to the modern technology of chemoinformatics which initially portrays the safety and toxicity profile of every compound. Otherwise investigating the ADMET through in-vivo are time and cost-effective and faces compound quantity problems [48]. In our research, by the help of chemoinformatics, we have portrayed the ADMET profile and molecular docking, simulations and in-silico cloning of our stress derived compounds.

As demonstrated by our research, all SMs (1–4, 6) have exhibited promising outcomes in both antibacterial activity and protein binding through molecular docking. Hence, it is imperative to focus on exploring the therapeutic significance of this process.

Conclusion and future perspectives

This study unveiled the potential benefits of metals-triggered compounds in combating pathogenic bacteria, suggesting their potential utility in addressing various diseases. The investigation employed in vitro experiments and computational tools to document pharmacological properties and predict bioactivities. Subsequent in vitro antibacterial screening of compounds revealed that the 5 stress metabolites (14, 6) exhibited remarkable antibacterial activity against *S. aureus*. Furthermore, transcriptomics and bioinformatics analysis was employed to elucidate the anti-*S. aureus* effects of SM-6 at the molecular level by regulating multiple desirable targets and pathways. It was found that SM-6 demonstrated its multifaceted impact on *S. aureus*, involving modulation of heat shock protein genes, disruption of protein folding and synthesis, interference with cellular redox balance, collectively resulting in the effective inhibition of normal bacterial growth. Furthermore, clinical investigations are essential to validate the outcomes of the current research. The limitations of this study is to still investigate the mechanism behind the heavy metals stress elicitation of the compounds in microorganisms. Nevertheless, the findings of this study will offer valuable insights for the future design and advancement of novel lead compounds as bioactive agents. All the old libraries of microorganisms can be re-evaluated by using heavy metals to investigate the sleeping genes activation through heavy metals and this technique may uncover some novel interesting compounds from microorganisms.

Abbreviations

RSM	Response surface methodology
ADMET	Absorption, distribution, metabolism, excretion, toxicity
TLR	Toll like receptor
PBP	Penicillin-binding protein
SM	Stress metabolite
HPLC	High-performance liquid chromatography
NMR	Nuclear magnetic resonance
BBD	Box-Behnken Design
UFF	Universal force field
MDS	Molecular docking simulations
CAI	Codon Adaptation Index
DEG	Differentially expressed genes
GO	Gene Ontology
BBB	Blood brain barrier

Supplementary Information

The online version contains supplementary material available at https://doi.org/10.1186/s12934-024-02573-0.

Supplementary material 1.

Acknowledgements
Not applicable.

Author contributions
S.S.U.H; paper writing and reviewing, experimental work, J.J.W; Transcriptomic data analyzing and paper writing, L.T; Supervision, paper reviewing, X.W.Y; sampling of bacteria and supervision, A.R; chemo informatics portion writing and data analyzing, H.Z.J; Project administration and supervision.

Funding
We are extremely grateful to the NSFC (81973191), Shanghai Agriculture Applied Technology Development Program, China (T20200104), and the National Key Research and Development Program of China (2018YFE0192600) for providing financial support for the complete undertaking.

Availability of data and materials
No datasets were generated or analysed during the current study.

Declarations

Ethics approval and consent to participate
Not applicable.

Consent for publication
All authors approved for publication.

Competing interests
The authors declare no competing interests.

Author details
[1]Shanghai Key Laboratory for Molecular Engineering of Chiral Drugs, School of Pharmacy, Shanghai Jiao Tong University, Shanghai 200240, People's Republic of China. [2]Shanghai Veterinary Research Institute, Chinese Academy of Agricultural Sciences, Shanghai 200241, People's Republic of China. [3]Key Laboratory of Pollution Exposure and Health Intervention of Zhejiang Province, Department of Basic Medical Sciences, Shulan International Medical College, Zhejiang Shuren University, Hangzhou, China. [4]College of Life Sciences, Northwest A&F University, Yangling, Xianyang 712100, People's Republic of China.

Received: 1 July 2024 Accepted: 29 October 2024
Published online: 12 November 2024

References

1. Hassan SS, Shaikh AL. Marine actinobacteria as a drug treasure house. Biomed Pharmacother. 2017;87:46–57.
2. Anjum K, Abbas SQ, Shah SAA, Akhter N, Batool S, Hassan SSU. Marine sponges as a drug treasure. Biomol Ther. 2016;24:347–62. https://doi.org/10.4062/biomolther.2016.067.
3. Anjum K, Abbas SQ, Akhter N, Shagufta BI, Shah SAA, Hassan SS. Emerging biopharmaceuticals from bioactive peptides derived from marine organisms. Chem Biol Drug Des. 2017. https://doi.org/10.1111/cbdd.12925.
4. Hassan SS, Anjum K, Abbas SQ, Akhter N, Shagufta BI, Shah SAA, et al. Emerging biopharmaceuticals from marine actinobacteria. Environ Toxicol Pharmacol. 2017. https://doi.org/10.1016/j.etap.2016.11.015.
5. Shams S, Abbas SQ, Muhammad I, Wu J, Yan S, Ali F, et al. Metals-triggered compound CDPDP exhibits anti-arthritic behavior by downregulating the in fl ammatory cytokines, and modulating the oxidative storm in mice models with extensive ADMET, docking and simulation studies. Front Pharmacol. 2022;13:1053744.
6. Wibowo JT, Bayu A, Aryati WD, Fernandes C, Yanuar A, Kijjoa A, et al. Secondary metabolites from marine-derived bacteria with antibiotic and antibiofilm activities against drug-resistant pathogens. Mar Drugs. 2023. https://doi.org/10.3390/md21010050.
7. Srinivasan R, Kannappan A, Shi C, Lin X. Marine bacterial secondary metabolites: a treasure house for structurally unique and effective antimicrobial compounds. Mar Drugs. 2021;19:530.
8. Weremfo A, Abassah-Oppong S, Adulley F, Dabie K, Seidu-Larry S. Response surface methodology as a tool to optimize the extraction of bioactive compounds from plant sources. J Sci Food Agric. 2023;103:26–36. https://doi.org/10.1002/jsfa.12121.
9. Zhang X, Hindra EMA. Unlocking the trove of metabolic treasures: activating silent biosynthetic gene clusters in bacteria and fungi. Curr Opin Microbiol. 2019. https://doi.org/10.1016/j.mib.2019.03.003.
10. Mohammadipanah F, Kermani F, Salimi F. Awakening the secondary metabolite pathways of promicromonospora kermanensis using physicochemical and biological elicitors. Appl Biochem Biotechnol. 2020. https://doi.org/10.1007/s12010-020-03361-3.
11. Hassan SS, Shah SAA, Pan C, Fu L, Cao X, Shi Y, et al. Production of an antibiotic enterocin from a marine actinobacteria strain H1003 by metal-stress technique with enhanced enrichment using response surface methodology. Pak J Pharm Sci. 2017;30:313–24.
12. Li J, Wang G, Yan B, Liu G. The responses of soil nitrogen transformation to nitrogen addition are mainly related to the changes in functional gene relative abundance in artificial Pinus tabulaeformis forests. Sci Total Environ. 2020;723:137679.
13. Caporaso JG, Kuczynski J, Stombaugh J, Bittinger K, Bushman FD, Costello EK, et al. QIIME allows analysis of high-throughput community sequencing data. Nat Methods. 2010;7:335–6. https://doi.org/10.1038/nmeth.f.303.
14. Magoč T, Salzberg SL. FLASH: fast length adjustment of short reads to improve genome assemblies. Bioinformatics. 2011;27:2957–63. https://doi.org/10.1093/bioinformatics/btr507.
15. Edgar RC. Search and clustering orders of magnitude faster than BLAST. Bioinformatics. 2010;26:2460–1. https://doi.org/10.1093/bioinformatics/btq461.
16. Wang Q, Garrity GM, Tiedje JM, Cole JR. Naïve Bayesian classifier for rapid assignment of rRNA sequences into the new bacterial taxonomy. Appl Environ Microbiol. 2007. https://doi.org/10.1128/AEM.00062-07.
17. Daina A, Michielin O, Zoete V. SwissADME: A free web tool to evaluate pharmacokinetics, drug-likeness and medicinal chemistry friendliness of small molecules. Sci Rep. 2017;7:1–13.
18. Braga RC, Alves VM, Silva MFB, Muratov E, Fourches D, Lião LM, et al. Pred-hERG: a novel web-accessible computational tool for predicting cardiac toxicity. Mol Inform. 2015;34:698–701.
19. Shams ul Hassan S, Qamar Abbas S, Ali F, Ishaq M, Bano I, Hassan M, et al. A comprehensive in silico exploration of pharmacological properties, bioactivities, molecular docking, and anticancer potential of vieloplain F from Xylopia vielana targeting B-Raf Kinase. Molecules. 2022;27:917.
20. Ferreira LG, Dos Santos RN, Oliva G, Andricopulo AD. Molecular docking and structure-based drug design strategies. Molecules. 2015;20:13384–421.
21. Emwas A-H, Roy R, McKay RT, Tenori L, Saccenti E, Gowda GAN, et al. NMR spectroscopy for metabolomics research. Metabolites. 2019. https://doi.org/10.3390/metabo9070123.
22. Wei J, Zhang XY, Deng S, Cao L, Xue QH, Gao JM. α-Glucosidase inhibitors and phytotoxins from streptomyces xanthophaeus. Nat Prod Res. 2017;31:2062–6. https://doi.org/10.1080/14786419.2016.1269100.
23. Perry JA, Koteva K, Verschoor CP, Wang W, Bowdish DM, Wright GD. A macrophage-stimulating compound from a screen of microbial natural products. J Antibiot. 2015;68:40–6. https://doi.org/10.1038/ja.2014.83.
24. Duarte N, Ferreira MJU. Lagaspholones A and B: two new jatropholane-type diterpenes from euphorbia iagascae. Org Lett. 2007;9:489–92.
25. Lu C, Xie F, Shan C, Shen Y. Two novel cyclic hexapeptides from the genetically engineered Actinosynnema pretiosum. Appl Microbiol Biotechnol. 2017;101:2273–9.
26. Bian- SUN. Chemical constituents of onchidium struma from chongming island shanghai. Nat Prod Res Dev. 2014;26:7–10.
27. Ul Hassan SS, Muhammad I, Abbas SQ, Hassan M, Majid M, Jin HZ, et al. Stress driven discovery of natural products from actinobacteria with antioxidant and cytotoxic activities including docking and admet properties. Int J Mol Sci. 2021;22:1–19.
28. Calloni G, Chen T, Schermann SM, Chang H, Genevaux P, Agostini F, et al. DnaK functions as a central hub in the E. coli chaperone network. Cell Rep. 2012;1:251–64.
29. Poehlsgaard J, Douthwaite S. The bacterial ribosome as a target for antibiotics. Nat Rev Microbiol. 2005;3:870–81. https://doi.org/10.1038/nrmicro1265.
30. Schäfer H, Heinz A, Sudzinová P, Voß M, Hantke I, Krásný L, et al. Spx, the central regulator of the heat and oxidative stress response in B. subtilis, can repress transcription of translation-related genes. Mol Microbiol. 2019;111:514–33. https://doi.org/10.1111/mmi.14171.
31. Shams S, Zhang W, Jin H, Basha SH, Priya SVSS. In-silico anti-inflammatory potential of guaiane dimers from Xylopia vielana targeting COX-2. J Biomol Struct Dyn. 2020;40:484–98. https://doi.org/10.1080/07391102.2020.1815579.
32. Shams Hassan S, Abbas SQ, Hassan M, Jin H-Z. Computational exploration of anti-cancer potential of guaiane dimers from xylopia vielana by targeting B-Raf kinase using chemo-informatics, molecular docking and MD simulation studies. Anticancer Agents Med Chem. 2022;22:731–46.
33. Daina A, Zoete V. A BOILED-egg to predict gastrointestinal absorption and brain penetration of small molecules. ChemMedChem. 2016. https://doi.org/10.1002/cmdc.201600182.
34. Chen Y, Tian Y, Gao Y, Wu F, Luo X, Ju X, et al. In silico design of novel HIV-1 NNRTIs based on combined modeling studies of dihydrofuro[3,4-d]pyrimidines. Front Chem. 2020. https://doi.org/10.3389/fchem.2020.00164.
35. Okem A, Stirk WA, Street RA, Southway C, Finnie JF, Van Staden J. Effects of Cd and Al stress on secondary metabolites, antioxidant and antibacterial activity of Hypoxis hemerocallidea Fisch. & C.A. Mey Plant Physiol Biochem. 2015;97:147–55.
36. Shams Hassan S, Jin H, Abu-Izneid T, Rauf A, Ishaq M, Suleria HAR. Stress-driven discovery in the natural products: a gateway towards new drugs. Biomed Pharmacother. 2019. https://doi.org/10.1016/j.biopha.2018.10.173.
37. Ul Hassan SS, Muhammad I, Abbas SQ, Hassan M, Majid M, Jin HZ, et al. Stress driven discovery of natural products from actinobacteria with antioxidant and cytotoxic activities including docking and admet properties. Int J Mol Sci. 2021;22:11432.
38. Ye P, Shen L, Jiang W, Ye Y, Chen CTA, Wu X, et al. Zn-driven discovery of a hydrothermal vent fungal metabolite clavatustide C, and an experimental study of the anti-cancer mechanism of clavatustide B. Mar Drugs. 2014;12:3203–17.
39. Raytapadar S, Datta R, Paul AK. Effects of some heavy metals on growth, pigment and antibiotic production by Streptomyces galbus. Acta Microbiol Immunol Hung. 1995;42:171–7.
40. Biswas R, Halder U, Kabiraj A, Mondal A, Bandopadhyay R. Overview on the role of heavy metals tolerance on developing antibiotic resistance in both Gram-negative and Gram-positive bacteria. Arch Microbiol. 2021;203:2761–70.
41. Shi Y, Pan C, Auckloo BN, Chen X, Chen CTA, Wang K, et al. Stress-driven discovery of a cryptic antibiotic produced by Streptomyces sp. WU20 from Kueishantao hydrothermal vent with an integrated metabolomics

strategy. Appl Microbiol Biotechnol. 2017;101:1395–408. https://doi.org/10.1007/s00253-016-7823-y.
42. Akhter N, Liu Y, Auckloo BN, Shi Y, Wang K, Chen J, et al. Stress-driven discovery of new angucycline-type antibiotics from a marine streptomyces pratensis NA-ZhouS1. Mar Drugs. 2018;16:1–16.
43. Hassan SS, Shah SAA, Pan C, Fu L, Cao X, Shi Y, et al. Stress driven discovery of natural products from actinobacteria with anti-oxidant and cytotoxic activities including docking and admet properties. Int J Mol Sci. 2021;22:11432.
44. Math HH, Kumar RS, Chakraborty B, Almansour AI, Perumal K, Kantli GB, et al. Antimicrobial Efficacy of 7-Hydroxyflavone derived from amycolatopsis sp. HSN-02 and its biocontrol potential on cercospora leaf spot disease in tomato plants. Antibiotics. 2023. https://doi.org/10.3390/antibiotics12071175.
45. Wu J, Hassan ul SS, Zhang X, Li T, Rehman A, Yan S, et al. Discovery of potent anti-MRSA components from Dalbergia odorifera through UPLC-Q-TOF-MS and targeting PBP2a protein through in-depth transcriptomic, in vitro, and in-silico studies. J Pharm Anal. 2024. https://doi.org/10.1016/j.jpha.2024.01.006.
46. Chakraborty B, Kumar RS, Almansour AI, Perumal K, Nayaka S, Brindhadevi K. Streptomyces filamentosus strain KS17 isolated from microbiologically unexplored marine ecosystems exhibited a broad spectrum of antimicrobial activity against human pathogens. Process Biochem. 2022;117:42–52.
47. Chakraborty B, Kumar RS, Almansour AI, Gunasekaran P, Nayaka S. Bioprospection and secondary metabolites profiling of marine Streptomyces levis strain KS46. Saudi J Biol Sci. 2022;29:667–79.
48. Medina-Franco JL, Sánchez-Cruz N, López-López E, Díaz-Eufracio BI. Progress on open chemoinformatic tools for expanding and exploring the chemical space. J Comput Aided Mol Des. 2022;36:341–54.

Publisher's Note